Experimental Study of Blasting Excavation for Large Cross-Section Tunnel in Horizontal Layered Rock Mass

Jie Mei
Geotechnical and Structural Engineering Research Center, Shandong University
Wanzhi Zhang (zwzwanzhi@163.com)
School of Transportation and Civil Engineering, Shandong Jiaotong University
Bangshu Xu
Geotechnical and Structural Engineering Research Center,Shandong University
Yongxue Zhu
China Railway Tunnel Group No.2 Co Ltd
Bingkun Wang
China Railway Tunnel Group No.2 Co Ltd

Original Paper

Keywords: large cross-section tunnel, horizontal layered rock mass, blasting excavation, field test, optimization of blasting parameters

Posted Date: February 9th, 2021

DOI: https://doi.org/10.21203/rs.3.rs-180296/v1

Experimental study of blasting excavation for large cross-section tunnel in horizontal layered rock mass

Jie Mei [1], Wanzhi Zhang [2]*, Bangshu Xu [1], Yongxue Zhu [3], Bingkun Wang [3]

[1] Geotechnical and Structural Engineering Research Center, Shandong University, Jinan 250061, China

[2] School of Transportation and Civil Engineering, Shandong Jiaotong University, Jinan 250357, China

[3] China Railway Tunnel Group No. 2 Co Ltd, Langfang 065201, China

* CORRESPONDENCE: Wanzhi Zhang; Email: zwzwanzhi@163.com

Abstract The drilling and blasting method is still the main method in mountain tunnel excavation. For large cross-section tunnel in horizontal layered rock mass, tunnel blasting often causes serious overbreak and underbreak. In this study, blasting excavation tests of tunnel upper face were conducted and failure mechanisms of surrounding rocks with weak beddings and joints were analyzed based on the Panlongshan tunnel. Then, the blasthole pattern, the cut mode, a variety of peripheral holes, the charge structure and the maximum single-hole charge were optimized. Compared with the failure characteristics, overbreak and underbreak, and deformations of surrounding rocks before and after optimization, the latter was better in tunnel contour forming and surrounding rock stability. The results show that after optimization, the large-area separation of vault rock mass is solved, the step-like overbreak of spandrel rock mass is reduced and the large-size rock blocks and underbreak are avoided. The maximum linear overbreak of vault, spandrel, and haunch surrounding rocks is decreased by 42.3%, 53.7% and 45.1%, respectively. The underbreak at the bottom of the upper face is reduced from -111.5 to - 16.5 cm. The average overbreak area is decreased by 61.1%. In addition, the displacements after optimization finally converge to the smaller values. The arch crown settlement and the horizontal convergence of haunch are reduced by about 21.6% and 18.3%, respectively. Furthermore, from the completion of blasting excavation to the stabilization of surrounding rock, it takes less time by using the optimized blasting scheme.

Keywords large cross-section tunnel; horizontal layered rock mass; blasting excavation; field test; optimization of blasting parameters

1. Introduction

In railway, highway and subway engineering, advanced controlled blasting techniques are the most commonly used methods of tunnel excavation for rapid tunnelling (Adhikari et al. 1999; Fu et al. 2010; Costamagna et al. 2018). Smooth blasting is the most commonly used method and a kind of controlled blasting technique, which meets the design requirements of the smooth contour line by using fine blasting parameters and division and subsection millisecond blasting (Sumiya and Kato 2007; Mandal et al. 2008; Johansson and Ouchterlony 2013). For a smooth blasting design, the damage on surrounding rock is mainly influenced by the geotechnical conditions (e.g. discontinuous beddings and joints, and rock properties) and blasting parameters such as the blasthole pattern and the charge scheme (Ramulu et al. 2009; Johnson 2010). Since tunnel excavation in horizontal layered rock mass is subjected to a large number of bedding planes, there is difficulty in forming a smooth excavation line using smooth blasting. In fact, the propagation of explosion energy is greatly influenced by the weak structural planes (e.g. barrier and leakage), leading to large overbreak or even collapse of surrounding rock. Therefore, the influence of weak structural planes on the smooth blasting excavation are required to be investigated systematically. Based on this, the protective blasting parameters to forming smooth tunnel contour line need to be proposed urgently.

In a tunnel face, according to the sequence of firing charges, the blasting excavation is occurred layer by layer from the center to the outside. First, the cut blasting occurs to break rock mass and throw broken stones to create a new free surface. Then, the relief blasting is carried out step by step to form larger blasting cavity. Finally,

the smooth blasting is conducted to create a smooth contour line. To date, many researches related to fine blasthole patterns and charge schemes for decreasing overbreak have been carried out. Shuifer and Azarkovich (1982) proposed the maximum permissible linear mass of the contour charge through formula derivation. Hinzen (1998) carried out a comparison between the measured seismic energy and the total explosive energy based on five smooth production blasting tests and claimed that the explosive performance and electronic initiation system contributed to the success of the smooth contour. Li et al. (2017) studied the smooth blasting fracture mechanisms from the timing sequence control techniques. Taking into account the specified control indices, including the arch crown settlement, thickness of the blasting damage zone, Liu and Liu (2017) put forward an intelligent optimization method of smooth blasting parameters for mountain tunnels by using a GA and ISVR coupling algorithm. Salum and Murthy (2019) suggested overbreak control methods by means of optimizing blasthole distance and the thickness of smooth blasting rock layer, as well as the charge of peripheral hole.

Tunnel excavation in the horizontal layered rock mass is highly influenced by the complex weak structural planes (Solak 2009; Deng et al. 2014). Some related studies indicate that under this geological structure, the explosive stress wave will be blocked from the structural planes, causing damage to the remaining rock mass out of excavation contour. Li and Ma (2009) employed an experimental technique to study the stress wave propagation across jointed rock mass and found that the joint width has a significant effect on the dynamic behavior of rock mass. Xie et al. (2016) developed the compression-shear damage model by considering damage patterns of rock mass and presented that the superposition of stress wave and the reflected tension waves from free surfaces contribute to the rock damage by using the finite element program. Deng et al. (2017) analyzed the mechanism of horizontal bedding in the process of propagation of explosive stress wave and theoretically explained the causes for overbreak on vault rock of tunnel.

Although there are many studies focused on the overbreak control for tunnels in jointed rock mass by proper blasting parameters design. Unfortunately, as a result of the complexity of influencing factors of tunnel blasting excavation and lack of understanding of the weak structural planes, there are no specific criterions and methods to determining the fine blasting parameters. For the large cross-section tunnel in the horizontal layered rock mass, it is necessary to study the practical blasting parameters in terms of the combined actions of horizontal beddings and joints and failure mechanism of surrounding rock. In this study, the Panlongshan tunnel project of the Taian-Feicheng expressway in the Shandong province of China was taken as an engineering case. The damage characteristics and overbreak of surrounding rock under the original blasting scheme (without taking into account the impact of bedding and joints) are first collected. Then, the mechanism analysis of weak structural planes on smooth blasting results was conducted and the causes of the severe overbreak are discussed systematically. Finally, the optimized controlled blasting parameters for tunnel excavation are proposed, and the applicability is proved by the next field blasting tests.

2. Panlongshan tunnel project

2.1 Engineering background and excavation method

The Panlongshan tunnel is a two-way separation-type tunnel located in the Taian-Feicheng expressway in the Shandong province of China. The lengths of the left and right tunnels are 2885 and 2875 m, respectively. The maximum cover depth of the tunnel is 160 m. Details of the tunnel engineering parameters and surrounding rock classifications are listed in Table 1. The surrounding rock of the tunnel is dolomitic intermediary weathered limestone with horizontal layered structure. The strike direction of the beddings is approximately parallel to the

axial direction of the tunnel. The geological longitudinal section along the tunnel axis is shown in Fig. 1. Remarkably, joints and fissures are also developed in the rock mass, which are filled with mud.

As shown in Fig. 2, the width and height of the standard cross-section of Class-IV surrounding rock are 17.56 and 12.44 m, respectively.

[Table 1 near here]

[Figure 1 near here]

[Figure 2 near here]

Bench excavation method is used in the Class-IV surrounding rock. According to the field investigation and monitoring measurement, overbreak and underbreak often occurs in the upper face due to the large excavation section (see Fig. 3). Therefore, the blasting excavation tests are carried out on the upper face. The excavation width, height, and area of the upper face are about 17.0 m, 7.5 m, and 101.3 m^2, respectively.

[Figure 3 near here]

2.2 Blasting scheme of the upper face

2.2.1 Blasthole pattern

As shown in Fig. 3, the face is divided into three sub-sections based on the structure of the drilling and blasting platform. As shown in Fig. 4(a), the sections A, B and C are the areas of wedge cutting blasting, relief blasting and smooth blasting, respectively. The timing sequence of the blasting is from A to B to C. Fig. 4(b) presents the design of the blasthole pattern and its parameters. The diameter of the holes is 42 mm, the length of each round excavation is about 4.0 m and the electronic detonator series are from 1 to 15. Since the width of the cutting blasting is about 8 m, in order to form an ideal cavity, the four-wedge cutting design is adopted. The spacing of one-wedge cut holes is 0.6 m and that of the two-, three- and four-wedge cut holes is around 0.9 m. The lengths and angles of these cut holes are 5.8, 5.0, 4.5 and 4.2 m, and 47°, 55°, 64° and 73°, respectively.

Due to the large free surface, the spacing of peripheral holes is 0.65 m at the vault and spandrel. In order to effectively release the constraint of remained rock mass, the spacing of peripheral holes is 0.55 m at the haunch. The thicknesses of smooth blasting rock layers are about 0.7 m at the vault and spandrel, and 0.8 m at the haunch. In addition, in order to weaken the influence of horizontal beddings, the interval layout of long holes and short holes of peripheral holes is used. Fig.5. shows the design parameters of the long hole and short hole. The distances of the long hole and short hole move inward from the contour is 20 and 14 cm, respectively. The lengths and look-out angles of the long hole and short hole are 4.0 and 2.0 m, and 5°and 8°, respectively.

Along the direction of the contour, the relief holes are distributed between the cut holes and peripheral holes and are drilled in a staggered manner. The spacing of the relief holes are 1.0~1.5 m at the vault and spandrel, and 0.8~0.9 m at the haunch.

The bottom holes are located at the interface between the upper and lower faces with a distance about 1.3 m.

[Figure 4 near here]

[Figure 5 near here]

2.2.2 Charge and blasting network

The emulsion explosive with a diameter of 32 mm and a length of 0.3 m is used. The explosive density is 1125 kg/m^3 and the velocity of detonation is 3200 m/s. The uncoupled charge with an uncoupled coefficient of

1.31 is used in the transverse direction, whereas in the longitudinal direction, the concentrated charge at the bottom of blasthole is adopted.

A typical millisecond-delay blasting sequence is used. The cut holes are firstly detonated, followed by the relief holes and the peripheral holes with delay intervals of 50 ~ 100 ms. The delay time is controlled by electronic detonators in odd series (see Fig. 3). The blastholes in the vault are divided into left, middle and right parts, and each part is clustered and detonated by detonators. The blastholes in the haunch is divided into left and right parts, and each part is clustered and detonated by detonators.

To sum up, the parameters of blastholes and charges of upper face are listed in Table 2.

[Table 2 near here]

2.3 Results of blasting excavation

2.3.1 Failure characteristics of surrounding rock

From ZK80+263.0 to ZK80+239.6, the left tunnel was excavated 6 times by using the above blasting scheme. The failure characteristics of surrounding rock after blasting excavation are shown in Fig. 6. It can be seen from the arch remaining rock mass (Fig.6a, b, c), discontinuous horizontal beddings and vertical joints are developed. The bedding spacing ranges from a few centimeters to tens of centimeters. These joints are intersected with horizontal beddings, and the joints are filled with mud. Affected by the influence of horizontal beddings and joints, the surrounding rock was badly damaged and the tunnel contour was very irregular. The vault rock mass fell off along a bedding plane, forming a flat outline. At the spandrel, broken rocks slid down along a joint plane, leading to a distinct step-like outline. The maximum height and width of step-like rock fracture surface were 72 and 34 cm.

It could be seen from the bottom remaining rock mass (Fig.6d, e), the face was roughness and there was underbreak at the bottom. Because the distance of the one-wedge cut holes on the face was about 8.0 m, the cutting blasting generated large-size stone. The length, width, and height of the stone was about 1.8 m × 1.0 m × 1.4 m. In order to realize the transportation of large-size stone, it was necessary to carry out secondary drilling and blasting.

[Figure 6 near here]

2.3.2 Overbreak and underbreak

The Leica TCA total station and the BJSD-3 tunnel section laser were used to measure the length of each round excavation, deformation of surrounding rock, overbreak and underbreak, as shown in Fig. 7.

The quantitative sizes of overbreak and underbreak of the test sections ZK80+254.2 and ZK80+250.4 are shown in Fig. 8. It could be seen that the overbreak of the tunnel vault and spandrel after blasting excavation was serious, and there was local underbreak at the middle and bottom of the upper face. The maximum linear overbreak of the vault, spandrel and haunch were 39.0, 82.5 and 33.1 cm. The average overbreak area was 8.55 m^2. The maximum linear underbreak of the bottom was -111.5 cm. According to JTG F60-2009 (China First Highway Engineering Company Ltd 2009) standard, the permissible overbreak of the tunnel vault and side wall are 250 and 100 mm, and underbreak is not allowed in tunnel excavation. Therefore, overbreak of the vault, spandrel and haunch exceeded the standard value by 56.0%, 230.0% and 32.4%, respectively.

The average length of each round excavation was 3.65 m. An average blasting efficiency of 91.3 % had been achieved.

[Figure 7 near here]

[Figure 8 near here]

2.4 Analysis of tunnel contour forming mechanism of horizontal layered rock mass

2.4.1 Barrier effect of beddings on stress wave propagation

When explosive stress wave passes through bedding or joint with a thickness of Δr, the reflection and transmission are illustrated in Fig. 9. It is assumed that the stress wave σ is incident from the interface A, then forms reflected wave σ_{R1} and transmitted wave σ_{T1} there. The transmitted wave σ_{T1} is repeatedly reflected and transmitted between interfaces A and B. A series of reflected waves σ_R and transmitted waves σ_T are formed, which are expressed as:

$$\sigma_T^1 = \varphi_{T12}\sigma\,,\ \ \sigma_R^1 = -\varphi_{R12}\sigma\,;$$

$$\sigma_T^2 = \varphi_{T21}\eta\sigma_T^1\,,\ \ \sigma_R^2 = -\varphi_{R21}\eta\sigma_T^1\,;$$

$$\sigma_T^3 = -\varphi_{T21}\eta\sigma_R^2\,,\ \ \sigma_R^3 = \varphi_{R21}\eta\sigma_R^2\,;$$

……

$$\sigma_T^n = (-1)^n\varphi_{T21}\eta\sigma_R^{n-1}\,,\ \ \sigma_R^n = (-1)^{n-1}\varphi_{R21}\eta\sigma_R^{n-1} \tag{1}$$

where C_1 and C_2 are the P-wave velocity of rock and bedding; ρ is the density; therefore, $(\rho_0 C)_1$ and $(\rho_0 C)_2$ indicate the wave impedance of rock and bedding, respectively; η is the attenuation coefficient of the stress wave as propagating through the bedding. The parameters φ_{T12} and φ_{R12} are the transmission and reflection coefficients as the wave entering from rock to bedding, while φ_{T21} and φ_{R21} are the transmission and reflection coefficients of the reverse incidence, which can be expressed as:

$$\varphi_{T12} = \frac{2(\rho_0 C)_2}{(\rho_0 C)_1 + (\rho_0 C)_2}\,,\ \ \varphi_{R12} = \frac{(\rho_0 C)_2 - (\rho_0 C)_1}{(\rho_0 C)_1 + (\rho_0 C)_2}\,;$$

$$\varphi_{T21} = \frac{2(\rho_0 C)_1}{(\rho_0 C)_1 + (\rho_0 C)_2}\,,\ \ \varphi_{R21} = \frac{(\rho_0 C)_1 - (\rho_0 C)_2}{(\rho_0 C)_1 + (\rho_0 C)_2} \tag{2}$$

The sum of the stress waves entering rock at interfaces A and B can be expressed as:

$$\sigma_A = \sigma_R^1 + \sigma_T^3 + \sigma_T^5 + \cdots + \sigma_T^n, n = 1,3,5\cdots$$

$$\sigma_B = \sigma_T^2 + \sigma_T^4 + \sigma_T^6 + \cdots + \sigma_T^n, n = 2,4,6\cdots \tag{3}$$

The general expressions can be obtained by substituting Eqs. 1 and 2 into Eq. 3:

$$\begin{aligned}\sigma_A = &-\frac{(\rho_0 C)_2 - (\rho_0 C)_1}{(\rho_0 C)_1 + (\rho_0 C)_2}\cdot\sigma + \\ &\frac{2(\rho_0 C)_1}{(\rho_0 C)_1 + (\rho_0 C)_2}\cdot\frac{2(\rho_0 C)_2}{(\rho_0 C)_1 + (\rho_0 C)_2}\cdot\frac{(\rho_0 C)_1 - (\rho_0 C)_2}{(\rho_0 C)_1 + (\rho_0 C)_2}\cdot \\ &\eta^2\cdot\sum_{i=2}^{n}\left[(-1)^m(\eta\cdot\frac{(\rho_0 C)_1 - (\rho_0 C)_2}{(\rho_0 C)_1 + (\rho_0 C)_2})^{2m}\right]\cdot\sigma,\end{aligned} \tag{4}$$

$$m = 0,1,2\cdots; n = 3,5,7\cdots; n = 2m+3$$

$$\sigma_B = \frac{2(\rho_0 C)_1}{(\rho_0 C)_1 + (\rho_0 C)_2} \cdot \frac{2(\rho_0 C)_2}{(\rho_0 C)_1 + (\rho_0 C)_2} \cdot \eta \cdot \left[1 + \sum_{i=4}^{n} (-1)^m (\eta \cdot \frac{(\rho_0 C)_1 - (\rho_0 C)_2}{(\rho_0 C)_1 + (\rho_0 C)_2})^{2m}\right] \cdot \sigma, \quad (5)$$

$$m = 1, 2, 3 \cdots; n = 4, 6, 8 \cdots; n = 2m + 2$$

According to Eqs. 4 and 5, the greater the difference of wave impedances between rock and bedding and the smaller the thickness of bedding, the stronger the barrier effect on the explosive stress wave. As reported by Peng (2018), if the stress wave was reflected and transmitted once within a bedding and the wave impedance ratio was $(\rho_0 C)_1/(\rho_0 C)_2 = 0.1$, only 33.1% of the stress wave passed through the bedding. The bedding spacing of surrounding rock in the test sections of the Panlongshan tunnel ranges from a few centimeters to tens of centimeters. Therefore, there are some weak beddings between two peripheral holes. Besides, the mud within the weak interlayer further strengthens the barrier effect on the explosive stress waves. As a result, more explosive energy propagates along the weak beddings, leading to the blasting fractures, and eventually resulting in severe overbreak.

[Figure 9 near here]

2.4.2 Separating, rotating and sliding down of unstable rock blocks

Affected by the cross cutting of beddings and joints and tunnel contour line, unstable rock blocks are formed in the arch of tunnel after excavation(Wu and Chen 2001; Zhang et al. 2012). In our previous work, the failure modes of the unstable rock blocks formed by the intersection of horizontal beddings and one or two sets of joints and the tunnel contour line were studied in detail by using the ubiquitous joint model embedded in FLAC3D (Zhang et al. 2020). Fig.10 shows the numerical model of tunnel. The surrounding rock contains horizontal beddings and two sets of joints (J1 and J2). Based on the geological exploration data and geotechnical tests, normal stiffnesses of 2.0×10^9 Pa/m and 1.1×10^9 Pa/m and shear stiffnesses of 0.8×10^9 Pa/m and 0.5×10^9 Pa/m were used to represent deformability of the beddings and joints, respectively. Fig. 11 shows the deformation and failure characteristics of the unstable rock blocks after the tunnel excavation. It could be seen from Fig. 11(a) that the unstable rock blocks at the vault separated along a horizontal bedding plane under pressures of vault rock load and rock gravity after excavation, causing overbreak. It could be seen from Fig. 11(b) that under the cross cutting of horizontal beddings and two sets of vertical joints, one side of the free face of the unstable rock blocks separated along a horizontal bedding plane, and the other side slid upward along a joint plane. Finally, the unstable rock blocks rotated and fell down, resulting in overbreak. It could be seen from Fig. 11(c) that under the cross cutting of horizontal beddings and two sets of intersecting joints, the unstable rock blocks either separated along a horizontal bedding plane, or slid down along a joint plane, leading to overbreak.

[Figure 10 near here]

[Figure 11 near here]

3. Optimization of blasting scheme

3.1 Optimization of blasthole pattern

Fig. 12 shows the optimized blasthole pattern and its parameters. In order to enlarge the cut cavity, prevent the underbreak at the bottom of the upper face, and avoid large-size stone produced by cutting blasting, the cutting design is changed to the layout of center holes and four-wedge cutting holes. The spacing of center holes and the

distance from the bottom boundary are 1.0 m. The spacing of one-wedge cut holes is 0.6 m and that of the two-, three- and four-wedge cut holes is around 0.9 m. The lengths and angles of these cut holes are 5.7, 4.9, 4.4 and 4.1 m, and 48°, 57°, 66° and 77°, respectively.

Given the barrier effect of weak structural planes on blasting load and the cross cutting of beddings and joints and the tunnel contour line, a variety of peripheral holes with empty holes, long holes and short holes are designed and drilled. According to the research (Li et al. 2018), total reflection occurs when the stress wave propagates to the surface of the empty hole due to the wave impedance ratio of rock to air is close to zero. The reflected wave is conducive to the tensile failure of the rock mass, resulting in the generation of blasting fractures. So the empty holes are added at the spandrel and their spacing is 0.6 m. In addition, according to the JTG F60-2009 standard and the research results (Singh and Xavier 2005; Dey and Murthy 2011; Xu et al. 2019), from soft to medium hard rock, the spacing of peripheral holes ranges from 0.3 to 0.6 m. Thus, the spacing of long holes and short holes was adjusted to 0.6 m. It's remarkable that due to the interval drilling of empty holes, long holes and short holes, the spacing of peripheral holes at the spandrel and haunch is determined as 0.3 m.

Fig. 13 presents the layout parameters of the optimized long hole and short hole. In order to decrease excessive rock damage caused by drilling, the look-out angles of the long hole and short hole are set to 3° and 5°, respectively. In addition, the distances of the long hole and short hole move inward from the contour is 15 and 12 cm, respectively. Therefore, the look-out distances from the bottom of the hole outside the contour line are decreased to 6 and 5 cm, respectively.

Furthermore, from the haunch to the bottom, due to the large excavation width, four relief holes are added, which are two rows, and are arranged symmetrically on the left and right sides. The horizontal spacing of relief holes is reduced from 0.8 to 0.7 m. At the tunnel vault and spandrel, the spacing of relief holes are adjusted to 1.0~1.3 m.

[Figure 12 near here]

[Figure 13 near here]

3.2 Optimization of charge and charge structure

First, in order to reduce the vibration of cut blasting, the maximum single-hole charge of cut hole is determined as the following formula:

$$q_c = \frac{q \cdot l \cdot S_c}{N_c} \tag{6}$$

where q represents explosive unit consumption, kg/m^3; l is the length of blasthole; S_c represents section area of cut cavity; N_c is the number of cut holes. S_c is expressed as

$$S_c = \frac{L \cdot (D+d)}{2} \tag{7}$$

where L is the length of one side of the cutting cavity, m; D is the maximum spacing of cutting holes, m; d is the spacing between the bottom of cut holes.

As shown in Fig. 12, $L = 0.6\times3$, $D = 7.8$, $d = 0.4$, $l = (4.1\times8 + 4.4\times8 + 4.9\times8 + 5.7\times16) / 40 = 4.96$ and $N_c = 40$, we can obtain $S_c = 7.38$ m^2. Since the test sections are the Class-IV surrounding rock, the Protodyakonov coefficient $f = 6$, according to empirical statistics, $q = 3.0$ kg/m^3. Based on the Eq.(6), $q_c = 2.7$ kg.

Second, according to the Salum and Murthy's research (Salum and Murthy 2019), the charge of peripheral holes is obtained as follows:

$$y = 0.57 \ln x + 0.26 \quad (8)$$

Where y represents charge of single peripheral hole, kg; x is the length of each round excavation, m. As shown in Fig 14, when x = 4.0 m, $y \approx 1.0$ kg.

[Figure 14 near here]

Third, the eccentric uncouple charge along the transverse direction and the air-deck charge along the longitudinal direction are adopted. Fig. 15 presents charge structures of peripheral holes at different positions. The emulsion explosives are divided into two segments of 0.2 and 0.1 m in length and placed separately in the holes. The detonating cord goes through the entire length of the holes. The opening of the holes was blocked with a length of 250 mm stemming.

Finally, the optimized parameters of blastholes and charges of upper face are given in Table 3.

[Figure 15 near here]

4. Result analysis and discussion

4.1 Failure characteristics of surrounding rock

From ZK80+235.7 to ZK80+216.7, the left tunnel was excavated 5 times by using the optimized blasting scheme. Fig. 16 presents the failure characteristics of surrounding rock after blasting excavation. It could be observed from Fig.16a, b, c, the unevenness of the excavated contour was significantly reduced compared with the results in Fig.6a, b, c. At the vault, the excavated contour was curved rather than flat. There was no large area of rock mass separation, only a few small-size broken rock blocks fell off. From spandrel to haunch, the excavated contour was jagged instead of the step-like shape. There was no massive unstable rock blocks sliding down. It could be seen from Fig.16d, e, the face was smooth, the bottom was flat and the sizes of the crushed stones were small. The length, width, and height of the largest stone was about 0.8 m × 0.5 m × 0.4 m. The above excavation results indicated that the optimized blasthole pattern and charge were practical.

[Figure 16 near here]

4.2 Overbreak and underbreak

The quantitative sizes of overbreak and underbreak of the test sections ZK80+235.7 and ZK80+220.1 are illustrated in Fig. 17. The excavated contour of the tunnel was in good agreement with the designed contour. The maximum linear overbreak at the vault, spandrel, and haunch was 22.5, 38.2, and 17.3 cm, respectively. The above results were decreased by 42.3%, 53.7% and 45.1% compared with the values in Fig. 8. The average overbreak area was 5.12 m^2, which was decreased by 61.1%. The underbreak at the bottom of the upper face was reduced to - 16.5 cm. The advantage was that the bottom was flat, which was conducive to the next tunnelling.

The average length of each round excavation was 3.76 m. An average blasting efficiency was 94.0%, which was increased by 2.7% through a comparison with the previous result.

[Figure 17 near here]

4.3 Surrounding rock deformation

During the process of blasting excavation, the cumulative displacements of surrounding rock of the vault and haunch before and after optimization are shown in Fig. 18. The displacement measurement was started right after the shotcrete. The results for 17 days shown that the growth rate of the displacements decreased continually and

finally tended to zero. After optimization, the displacements finally converged to the smaller values. After 15 days, before and after optimization, the vault crown settlements were about 24.5 and 19.2 mm respectively, as well as the horizontal convergences were about 17.5 and 14.3 mm respectively. Besides, there was a distinct inflection point in the curves after 5~7 days, and the appearance of the inflection point before optimization was delayed. It meant that from the completion of blasting excavation to the stabilization of surrounding rock, it took less time by using the optimized blasting scheme. So that the surrounding rock of the tunnel was safer after optimization.

[Figure 18 near here]

5. Conclusions

The blasting excavation tests are carried out based on the Panlongshan tunnel project in China. The failure characteristics, overbreak and underbreak, and deformations of the remaining rock mass have been analyzed, with the purpose of finding out the damage law of tunnel blasting in horizontal layered rock mass. The influence mechanisms of weak beddings and joints on the tunnel outline forming have been summarized as barrier of explosion stress wave propagation and separating, rotating and sliding down of unstable rock blocks formed by combined cutting. Measures, such as the layout of cut mode of "center holes and four-wedge cutting holes", a variety of peripheral holes of "empty holes, long holes and short holes", reducing the spacing of peripheral holes, drilling deviations and the thickness of smooth blasting rack layer, adding two rows of relief holes, changing the charge structures of peripheral holes, decreasing the maximum single-hole charge, etc., are proposed. Finally, the applicability of the optimized blasting parameters of tunnel excavation is verified through the field tests.

For tunnel blasting in horizontal layered rock mass, the layout of cut mode of "center holes and four-wedge cutting holes" and decreasing the maximum single-hole charge contribute to increase the volume of cut cavity, reduce underbreak and blasting vibration. The layout of peripheral holes of "empty holes, long holes and short holes", reducing spacing of blastholes and drilling deviations, and optimizing charge structure are conducive to reduce overbreak and restrain the separation of the vault rock mass. Thus, the unevenness of the excavation contour line is greatly reduced. The maximum linear overbreak of vault, spandrel, and haunch surrounding rocks is decreased by 42.3%, 53.7% and 45.1%, respectively. The underbreak at the bottom of the upper face is reduced from -111.5 to - 16.5 cm. The average overbreak area is decreased by 61.1%.

By using the optimized blasting scheme for tunnel excavation, the damage depth of surrounding rock is reduced and the stability is better. The displacements finally converge to the smaller values. The arch crown settlement and the horizontal convergence of haunch are reduced by about 21.6% and 18.3%, respectively. Furthermore, from the completion of blasting excavation to the stabilization of surrounding rock, it takes less time by using the optimized blasting scheme.

Author Contributions

J.M. (Jie Mei), W.Z. (Wanzhi Zhang) and B.X. (Bangshu Xu) conducted the field blasting tests and the optimization of smooth blasting scheme; J.M. performed the numerical experiments and wrote the original manuscript; W.Z. reviewed and revised the original manuscript; B.X. provided financial support; Y.Z. (Yongxue Zhu), and B.W (Bingkun Wang) carried out the field data monitoring.

Acknowledgments

This research was funded by the National Natural Science Foundation of China (grant numbers 50909056).

Conflicts of Interest

The authors declare no conflict of interest.

ORCID

Jie Mei: https://orcid.org/0000-0002-5041-6595

Wanzhi Zhang: https://orcid.org/0000-0002-4037-1741

Bangshu Xu: https://orcid.org/0000-0002-4104-5526

References

Adhikari GR, Babu AR, Balachander R, Gupta RN (1999) On the application of rock mass quality for blasting in large underground chambers. *Tunnelling and Underground Space Technology* 14(3):367-375, DOI: 10.1016/s0886-7798(99)00052-8

Costamagna E, Oggeri C, Segarra P, Castedo R, Navarro J (2018) Assessment of contour profile quality in D&B tunnelling. *Tunnelling and Underground Space Technology* 75(5):67-80, DOI: 10.1016/j.tust.2018.02.007

China First Highway Engineering Company Ltd (2009) Technical Specifications for Construction of Highway Tunnel JTG F60-2009. Standards Press of China: Beijing, China, 13-69 (in Chinese)

Deng XF, Zhu JB, Chen SG, Zhao ZY, Zhou YX, Zhao J (2014) Numerical study on tunnel damage subject to blast-induced shock wave in jointed rock masses. *Tunnelling and Underground Space Technology* 43:88-100, DOI: 10.1016/j.tust.2014.04.004

Deng XH, Chen JX, Luo YB (2017) Blasting control technology of horizontal stratified rock tunnel. *Journal of Chang'an University (Natural Science Edition)* 37(2):73-80 (in Chinese)

Dey K, Murthy VMSR (2011) Delineating rock mass damage zones in blasting from in-field seismic velocity and peak particle velocity measurement. *International Journal of Engineering, Science and Technology* 3(2):1-62

Fu YH, Li XB, Dong LJ (2010) Analysis of smooth blasting parameters for tunnels in deep damaged rock mass. *Rock and Soil Mechanics* 31(5):1420–1426 (in Chinese)

Hinzen KG (1988) Comparison of seismic and explosive energy in five smooth blasting test rounds. *International Journal of Rock Mechanics and Mining Sciences* 35(7):957-967, DOI: 10.1016/s0148-9062(98)00159-4

Johansson D, Ouchterlony F (2013) Shock wave interactions in rock blasting the use of short delays to improve fragmentation in model-scale. *Rock Mechanics and Rock Engineering* 46(1):1-8, DOI: 10.1007/s00603-012-0249-7

Johnson JC (2010) The Hustrulid bar – a dynamic strength test and its application to the cautious blasting of rock. Ph.D. Thesis, Department of Mining Engineering, University of Utah

Li XP, Huang JH, Luo Y, Chen PP (2017) A study of smooth wall blasting fracture mechanisms using the Timing Sequence Control Method. *International Journal of Rock Mechanics and Mining Sciences* 92:1-8, DOI: 10.1016/j.ijrmms.2016.12.001

Liu K, Liu B (2017) Optimization of smooth blasting parameters for mountain tunnel construction with specified control indices

365 based on a GA and ISVR coupling algorithm. *Tunnelling and Underground Space Technology* 70:363-374, DOI:
366 10.1016/j.tust.2017.09.007
367 Li JC, Ma GW (2009) Experimental study of stress wave propagation across a filled rock joint. *International Journal of Rock*
368 *Mechanics and Mining Sciences* 46:471-478, DOI:10.1016/j.ijrmms.2008.11.006
369 Li M, Zhu Z, Liu R, Liu B, Zhou L, Dong Y (2018) Study of the Effect of Empty Holes on Propagating Cracks under Blasting
370 Loads. International Journal of Rock Mechanics and Mining Sciences 103:186-194, DOI: 10.1016/j.ijrmms.2018.01.043
371 Mandal SK, Singh MM, Dasgupta S (2008) Theoretical concept to understand plan and design smooth blasting pattern.
372 *Geotechnical and Geological Engineering* 26(4):399-416, DOI: 10.1007/s10706-008-9177-4
373 Peng H (2018) Study on propagation of explosive stress wave in rock mass with layered joints. Master's thesis, School of Civil
374 Engineering and Architecture, Anhui University of Science and Technology, Anhui, China (in Chinese)
375 Ramulu M, Chakraborty A K, Sitharam T G (2009) Damage assessment of basaltic rock mass due to repeated blasting in a
376 railway tunnelling project – A case study. *Tunnelling and Underground Space Technology* 24(2):208-221, DOI:
377 10.1016/j.tust.2008.08.002
378 Sumiya F, Kato Y (2007) A study on smooth blasting technique using detonating cords. *Science and Technology of Energetic*
379 *Materials* 68(6):167-171
380 Shuifer MI, Azarkovich AE (1982) Determination of the parameters of smooth blasting for the preliminary contouring method.
381 *Hydrotechnical Construction* 16(5):259-267, DOI: 10.1007/bf01427808
382 Salum AH, Murthy VMSR (2019) Optimising blast pulls and controlling blast-induced excavation damage zone in tunnelling
383 through varied rock classes. *Tunnelling and Underground Space Technology* 85:307-318, DOI:10.1016/j.tust.2018.11.02
384 Solak T (2009) Ground behavior evaluation for tunnels in blocky rock masses. *Tunnelling and Underground Space Technology*
385 24(3):323–330, DOI: 10.1016/j.tust.2008.10.004
386 Singh SP, Xavier P (2005) Causes, impact and control of overbreak in underground excavations. *Tunnelling and Underground*
387 *Space Technology* 20(1):63-71, DOI: 10.1016/j.tust.2004.05.004
388 WU L, Chen JP (2001) Study on smooth-blasting results in jointed and fractured rock. *Journal of China University of*
389 *Geosciences* 12(2):145-149 (in Chinese)
390 Xie LX, Lu WB, Zhang QB, Jiang QH, Wang GH, Zhao J (2016) Damage evolution mechanisms of rock in deep tunnels
391 induced by cut blasting. *Tunnelling and Underground Space Technology* 58:257-270, DOI:10.1016/j.tust.2016.06.004
392 Xu B, Zhang W, Shi W, Hao G, Liu X, Mei J (2019) Experimental study of parameters of tunneling blasting in jointed layered
393 rock mass. *Journal of China University of Mining and Technology* 48(6):1248-1255 (in Chinese)
394 Zhang ZX, Xu Y, Kulatilake PHSW, Huang X (2012) Physical model test and numerical analysis on the behavior of stratified

rock masses during underground excavation. *International Journal of Rock Mechanics and Mining Sciences* 49:134-147, DOI:10.1016/j.ijrmms.2011.11.001

Zhang W, Xu B, Mei J, Yue G, Shi W (2020) A numerical study on mechanical behavior of jointed rock masses after tunnel excavation. *Arabian Journal of Geosciences* 13(11):416, DOI: 10.1007/s12517-020-05358-y

List of Figures

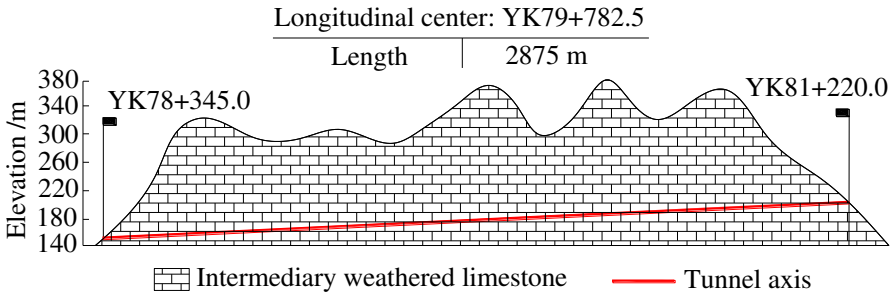

429

430 **Fig. 1** The geological longitudinal section of the Panlongshan tunnel

431

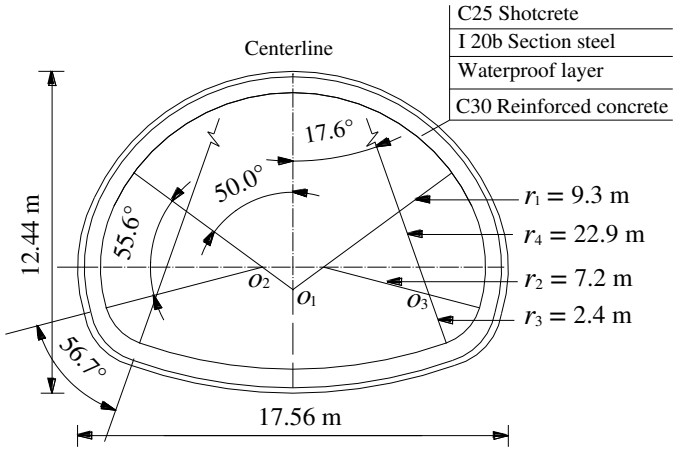

Fig. 2 The standard cross-section of the Class-IV surrounding rock

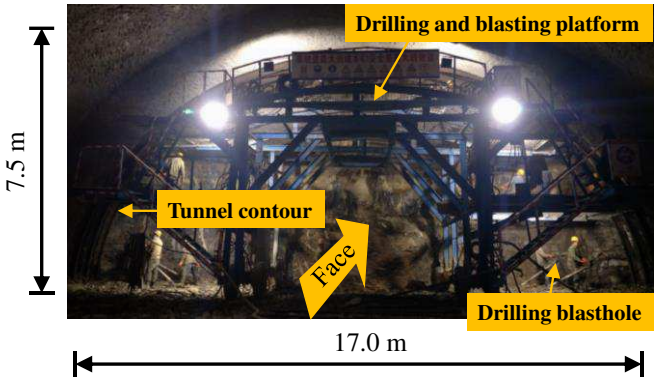

435

436 **Fig. 3** Scene of drilling and blasting excavation of the upper face

437

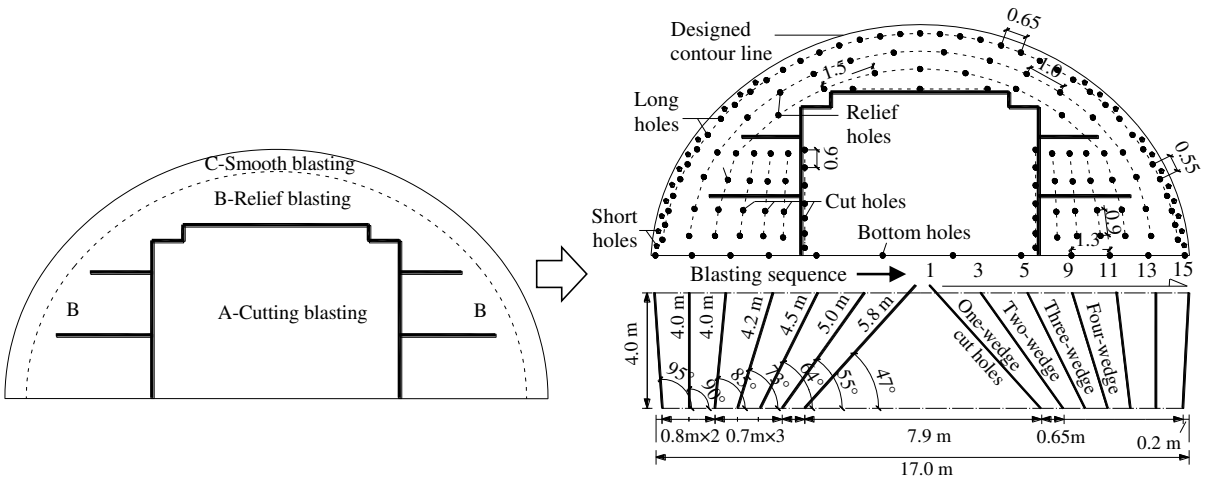

(a) (b)

Fig. 4 Blasthole pattern and detonator series of the upper face: (a) three sub-sections; (b) blasthole parameters

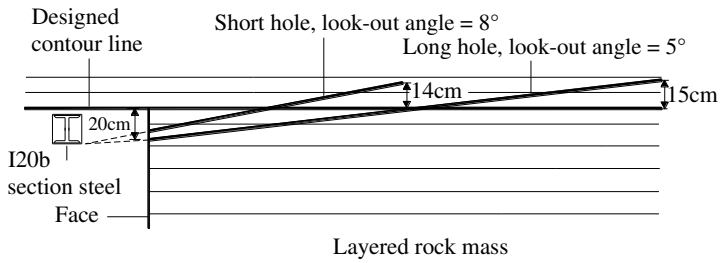

443

444 **Fig. 5** The layout of the long hole and short hole

445

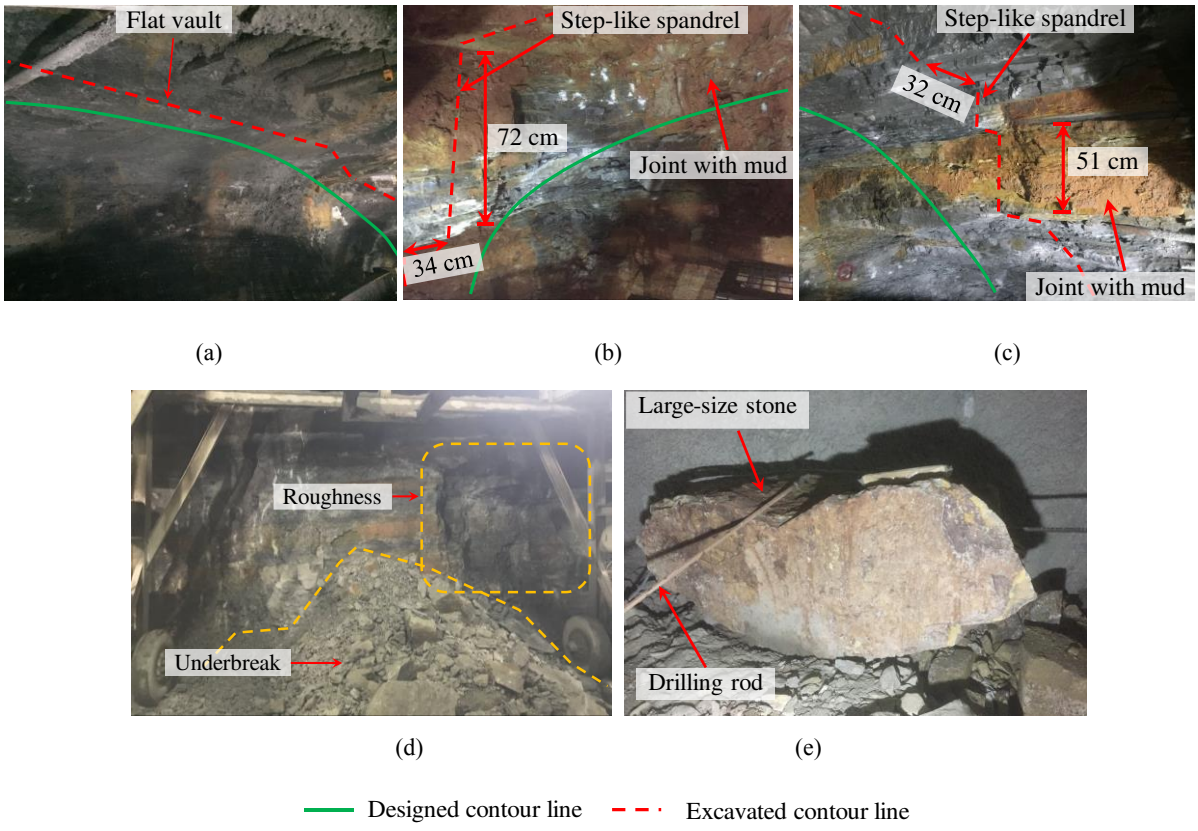

Fig. 6 The failure characteristics of horizontal layered surrounding rock after blasting excavation under the original blasting scheme: (a) vault, (b) left spandrel to haunch, (c) right spandrel to haunch, (d) rough face and underbreak, (e) large-size stone

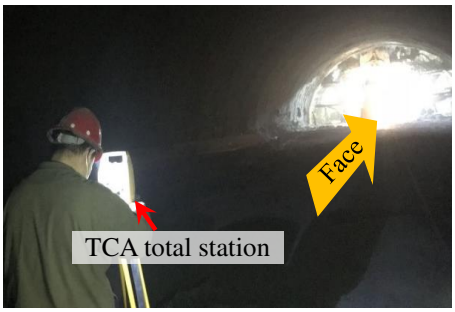

(a)

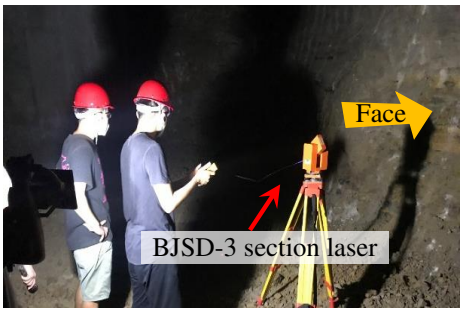

(b)

Fig. 7 Field measurements: (a) deformation of surrounding rock and length of each round excavation by using Leica TCA total station, (b) overbreak and underbreak by using BJSD-3 tunnel section laser

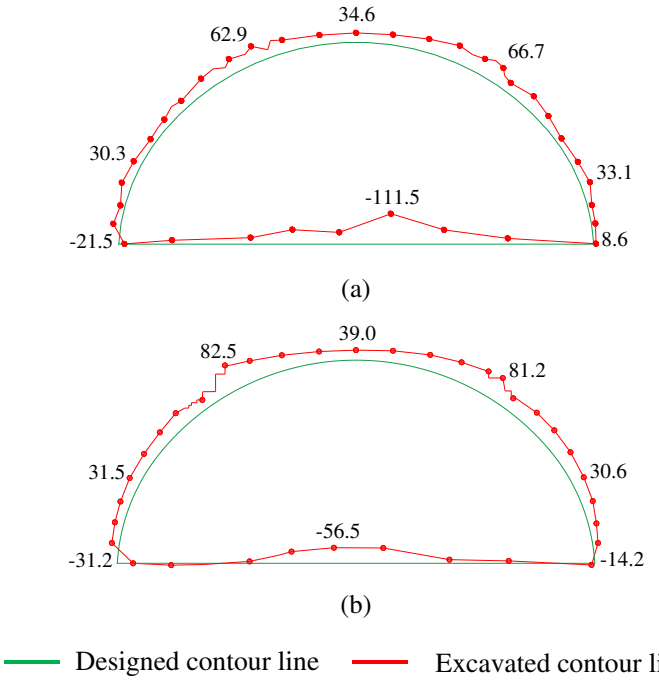

Fig. 8 Tunnel overbreak and underbreak of the test sections: (a) ZK80+254.2, (b) ZK80+250.4 (unit: cm)

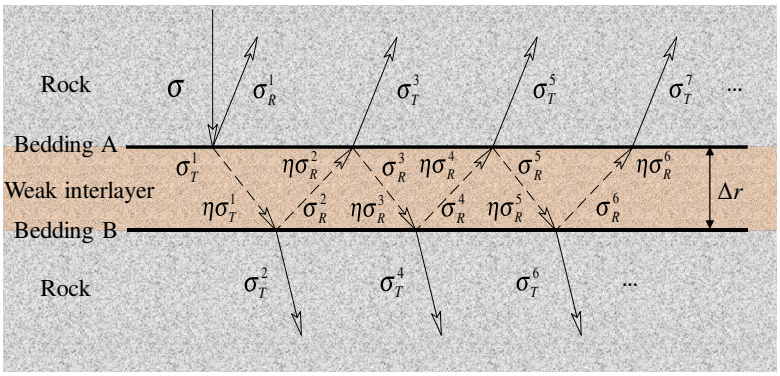

Fig. 9 Reflection and transmission of explosive stress wave passing through weak bedding

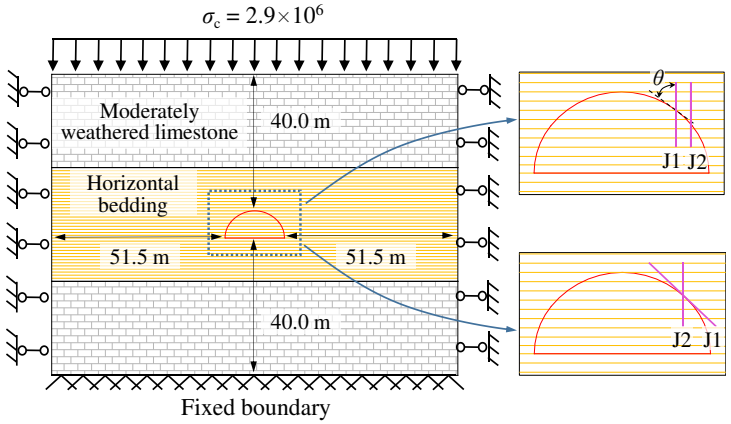

473

474 **Fig. 10** Numerical model of tunnel, and the surrounding rock contains horizontal beddings and two sets of joints

475

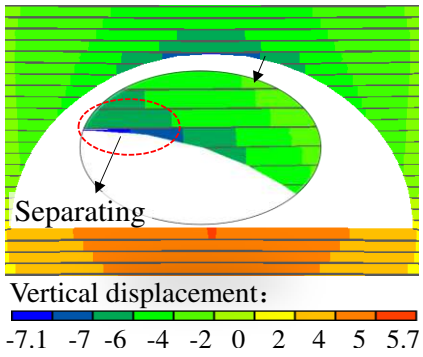

(a)

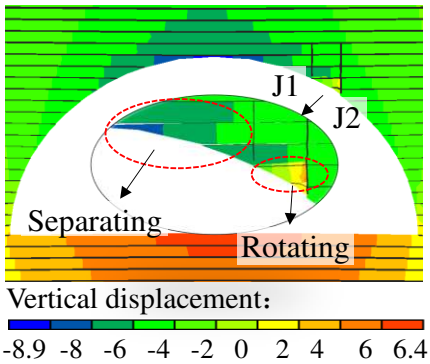

(b)

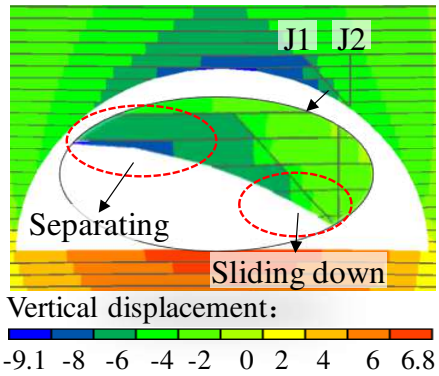

(c)

Fig. 11 Vertical deformations and failure modes after tunnel excavation: (a) surrounding rock with horizontal beddings, (b) surrounding rock with horizontal beddings and two parallel vertical joints, (c) surrounding rock with horizontal beddings and two sets of intersecting joints

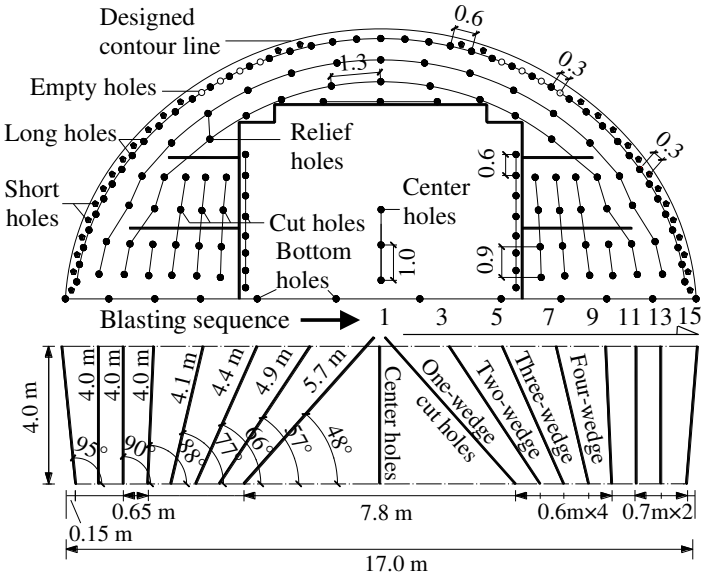

Fig. 12 The optimized blasthole pattern and detonator series of the upper face

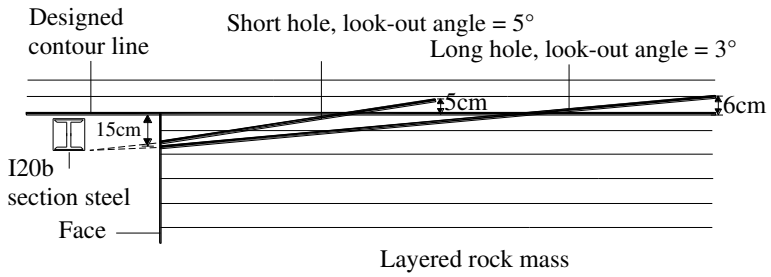

Fig. 13 The layout of the optimized peripheral holes

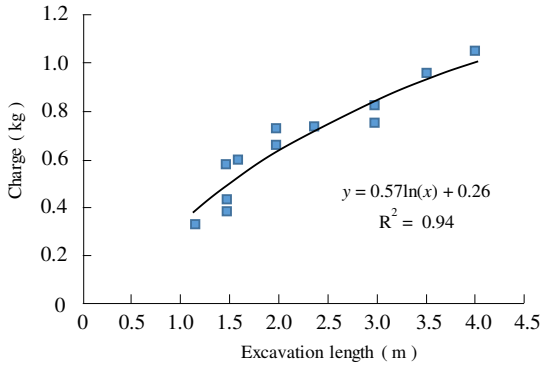

492

493 **Fig. 14** Relation between charge of peripheral hole and each round excavation length

494

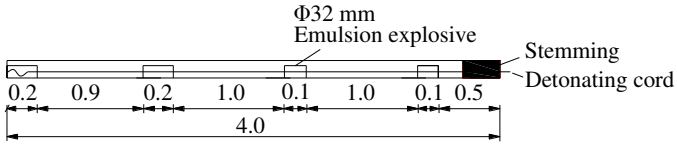

(a)

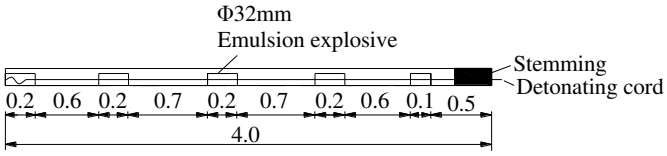

(b)

Fig. 15 The charge structures of peripheral holes: (a) vault and spandrel, (b) hance

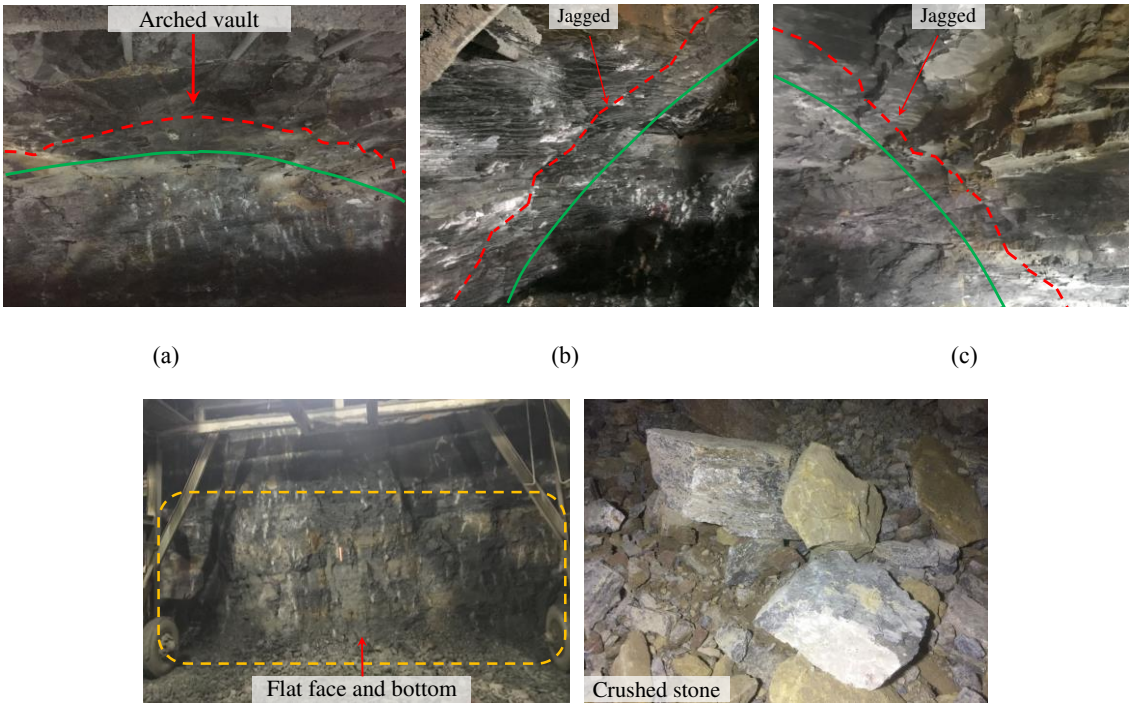

Fig. 16 The failure characteristics of horizontal layered surrounding rock after blasting excavation under the optimized blasting scheme: (a) vault, (b) left spandrel to haunch, (c) right spandrel to haunch, (d) flat face and bottom, (e) crushed stones

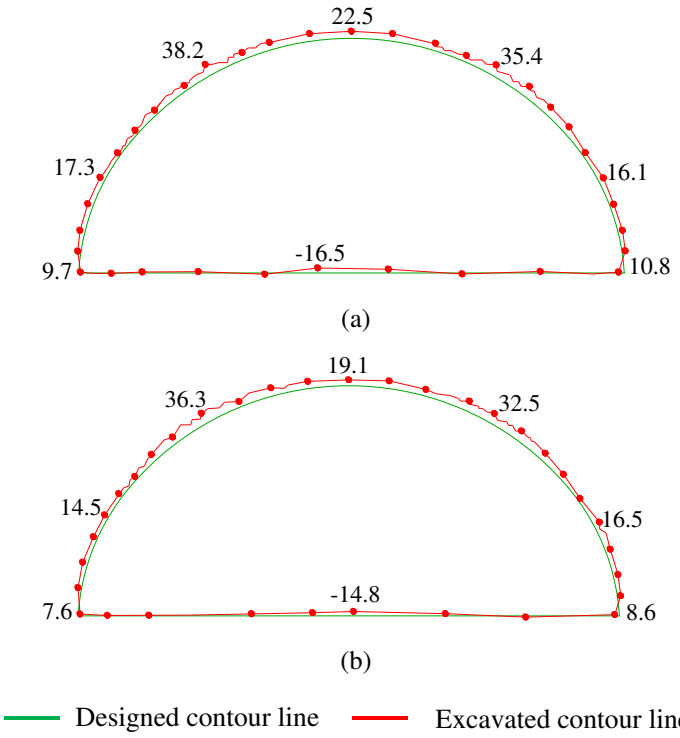

Fig. 17 Tunnel overbreak and underbreak of the test sections: (a) ZK80+235.7, (b) ZK80+220.1 (unit: cm)

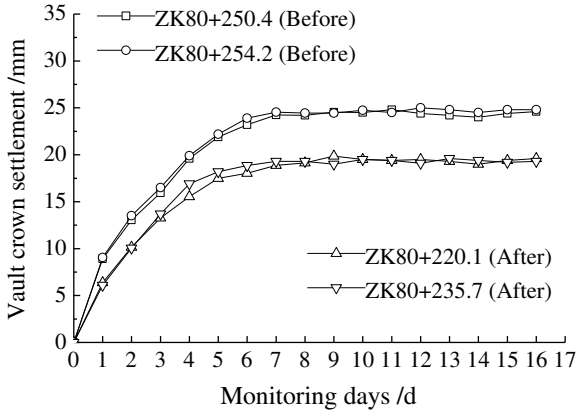

(a)

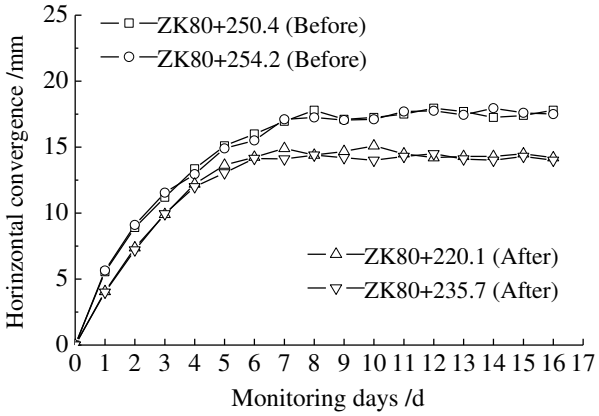

(b)

Fig. 18 The cumulative displacements of surrounding rock of the test sections: (a) vault crown settlement, (b) haunch horizontal convergence

List of Tables

529 **Table 1** Engineering parameters and surrounding rock classifications of the Panlongshan tunnel

Tunnel	Position		Length	Surrounding rock classification			Rock
	Entrance	Exit	(m)	Ⅲ(m)	IV(m)	V(m)	
Left	ZK78+345	ZK81+230	2885	1295	652	938	intermediary
Right	YK78+345	YK81+220	2875	971	997	907	weathered limestone

530

531

532 **Table 2** Tunnel blasthole and charge parameters of the upper face in the Class-IV surrounding rock

Position	Blast hole type	Detonator series	Delay time (ms)	Number of holes	Length (m)	Row spacing (m)	Charge (kg)	Total charge (kg)
Vault and spandrel	Long hole	15	880	23	4.0		0.6	13.8
	Short hole	15	880	6	2.0		0.3	1.8
	Buffer hole	13	650	10	4.0	0.60	0.9	9.0
		11	460	7	4.0	0.60	1.2	8.4
		9	310	3	4.0	0.65	1.5	4.5
Haunch	Long hole	15	880	16	4.0		0.9	14.4
	Short hole	15	880	16	2.0		0.3	3.6
	Buffer hole	13	650	8	4.0	0.80	1.2	9.6
		11	460	8	4.0	0.80	1.8	14.4
	Cut hole	9	310	8	4.2	0.70	2.1	16.8
		5	110	8	4.5	0.70	2.4	19.2
		3	50	8	5.0	0.70	2.7	21.6
		1	0	14	5.8	0.60	3.0	42.0
	Lifter hole	15	880	2	4.2		2.7	5.4
		13	650	4	4.2		2.7	10.8
		11	460	6	4.2		2.7	16.2
Sum				147				211.5

533

534

535 **Table 3** The optimized blasthole and charge parameters of the upper face in the Class-IV surrounding rock

Position	Blast hole type	Detonator series	Delay time (ms)	Number of holes	Length (m)	Row spacing (m)	Charge (kg)	Total charge (kg)
Vault and spandrel	Long hole	15	880	25	4.0		0.6	15
	Short hole	15	880	10	2.0		0.15	1.5
	Empty hole			8	4.0			
		13	650	11	4.0	0.60	0.9	9.9
	Buffer hole	11	460	9	4.0	0.60	0.9	8.1
		7	310	3	4.0	0.60	1.2	3.6
Hanch	Long hole	15	880	18	4.0		0.8	14.4
	Short hole	15	880	20	2.0		0.15	3.0
		13	650	8	4.0	0.70	1.2	9.6
	Buffer hole	11	460	8	4.0	0.70	1.5	12
		9	310	4	4.0	0.65	1.8	7.2
		7	200	8	4.1	0.60	1.8	14.4
	Cut hole	5	110	8	4.4	0.60	2.1	16.8
		3	50	8	4.9	0.60	2.4	19.2
		1	0	16	5.7	0.60	2.4	38.4
	Center hole	3	50	3	4.0		1.2/1.8/2.4	5.4
		15	880	2	4.2		2.4	4.8
	Lifter hole	13	650	4	4.2		2.4	9.6
		11	460	6	4.2		2.4	14.4
Sum				179				207.3

536

537

Figures

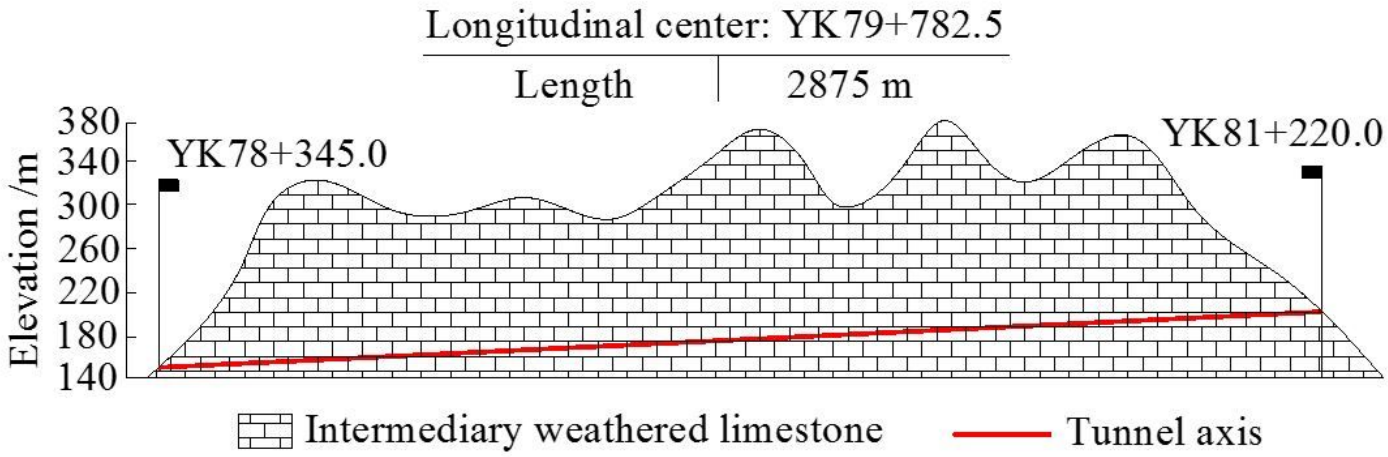

Figure 1

The geological longitudinal section of the Panlongshan tunnel

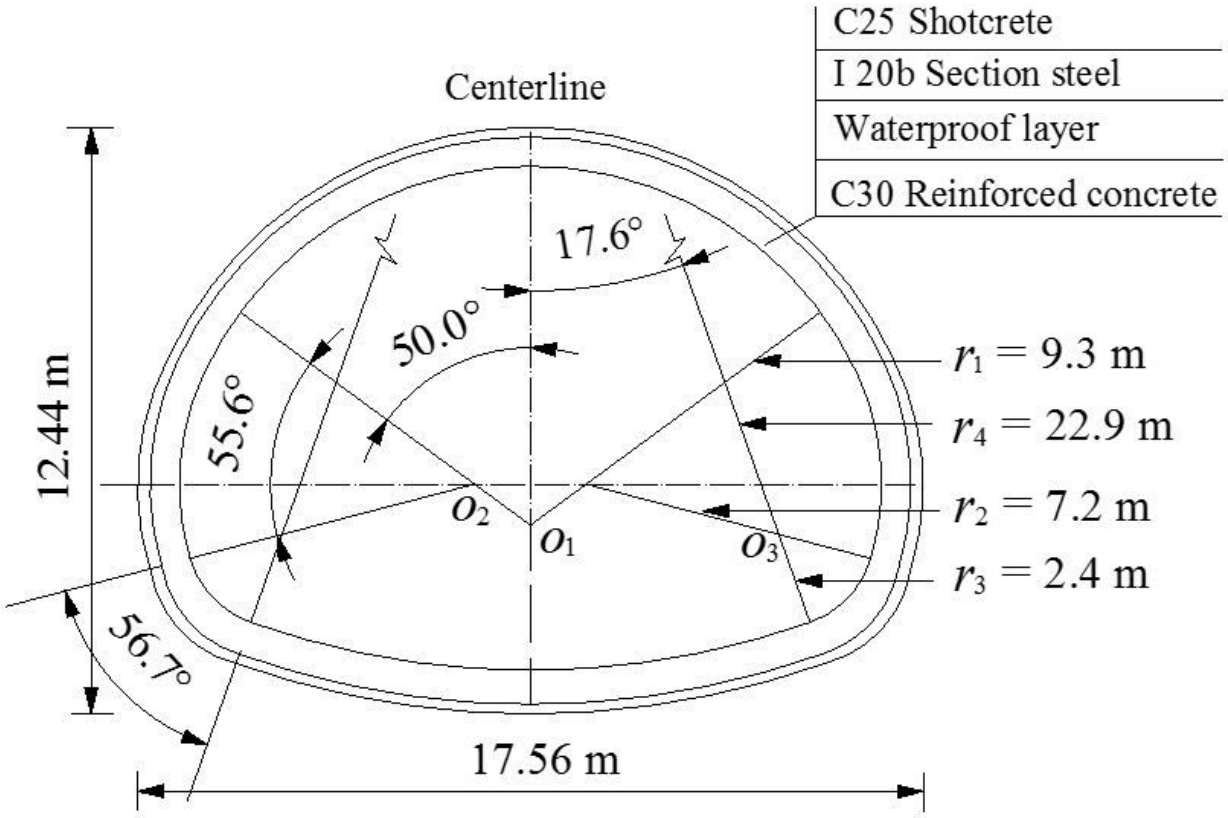

Figure 2

The standard cross-section of the Class-IV surrounding rock

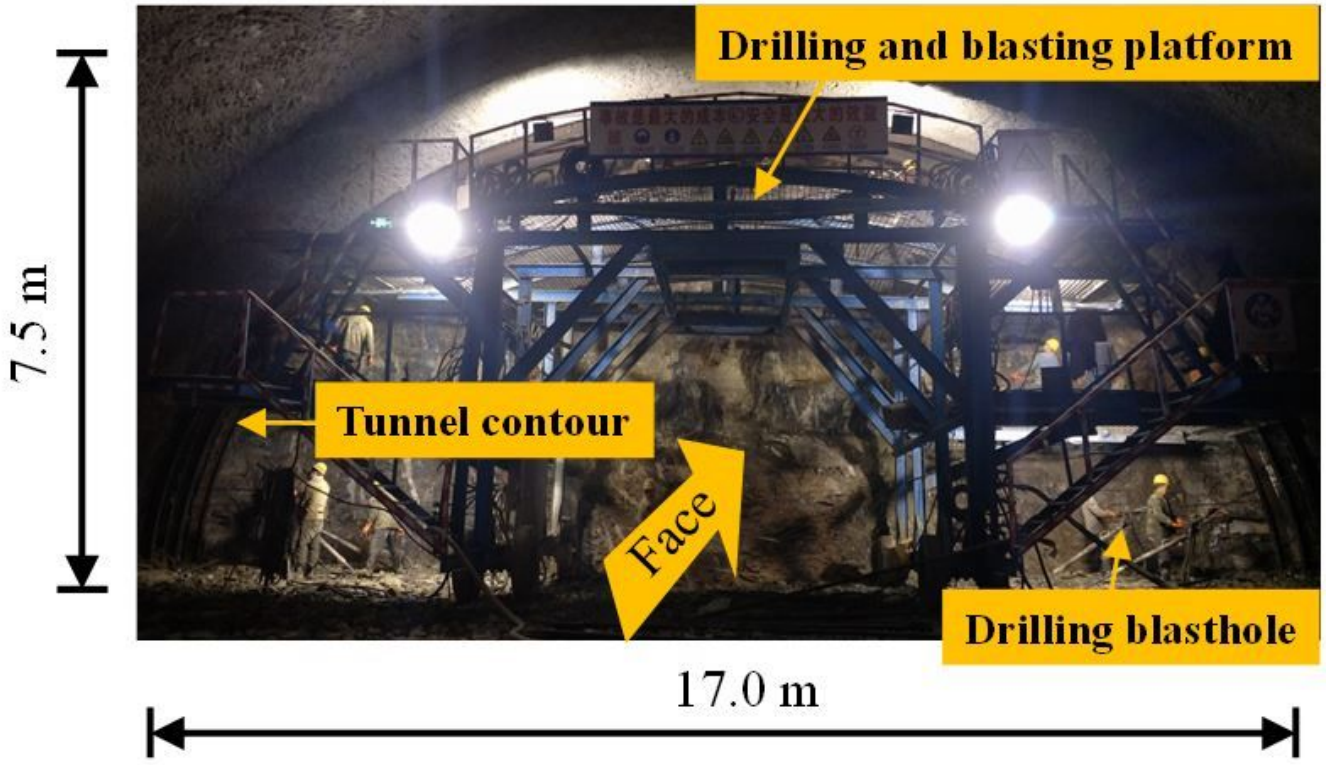

Figure 3

Scene of drilling and blasting excavation of the upper face

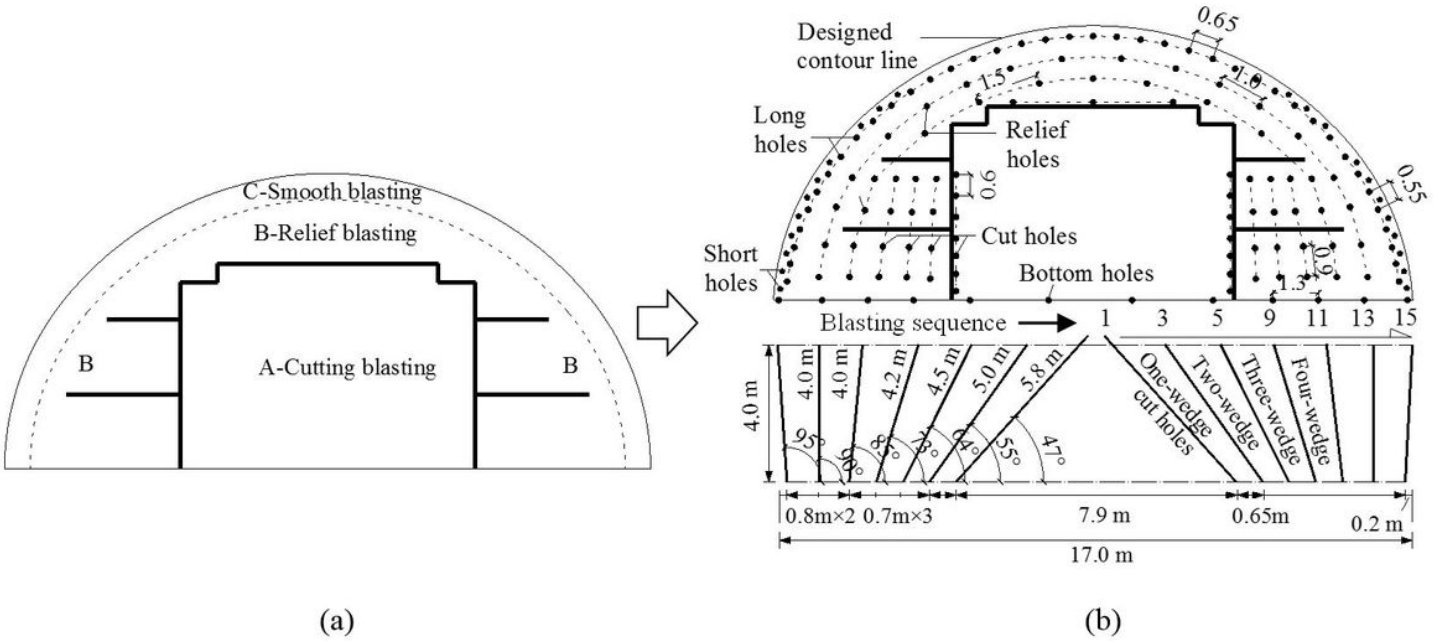

Figure 4

Blasthole pattern and detonator series of the upper face: (a) three sub-sections; (b) blasthole parameters

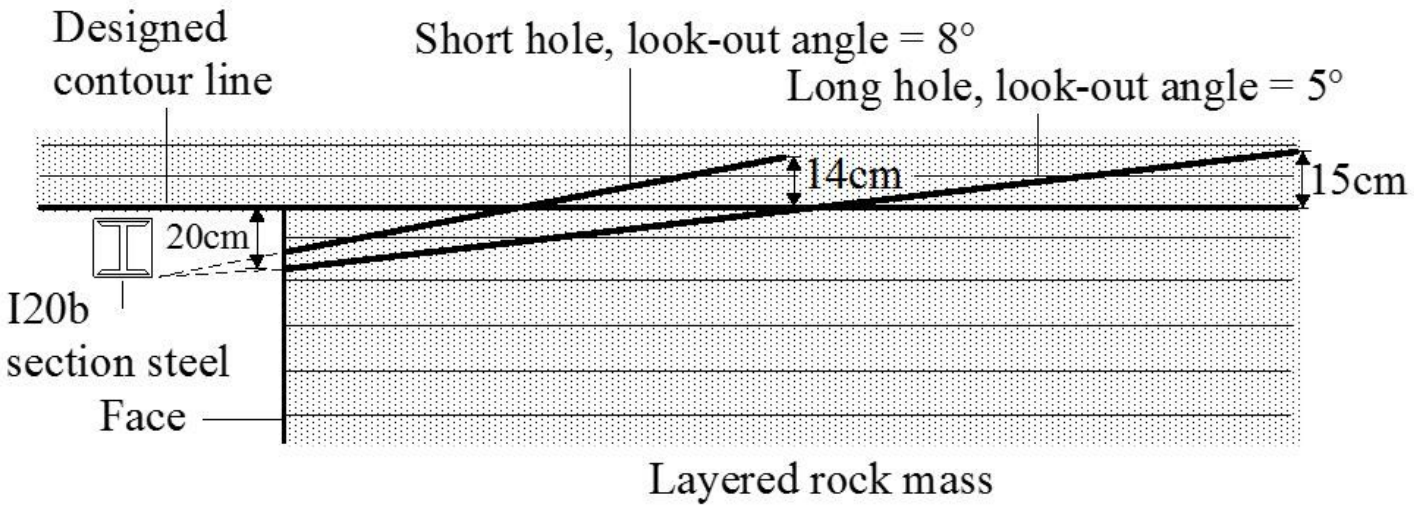

Figure 5

The layout of the long hole and short hole

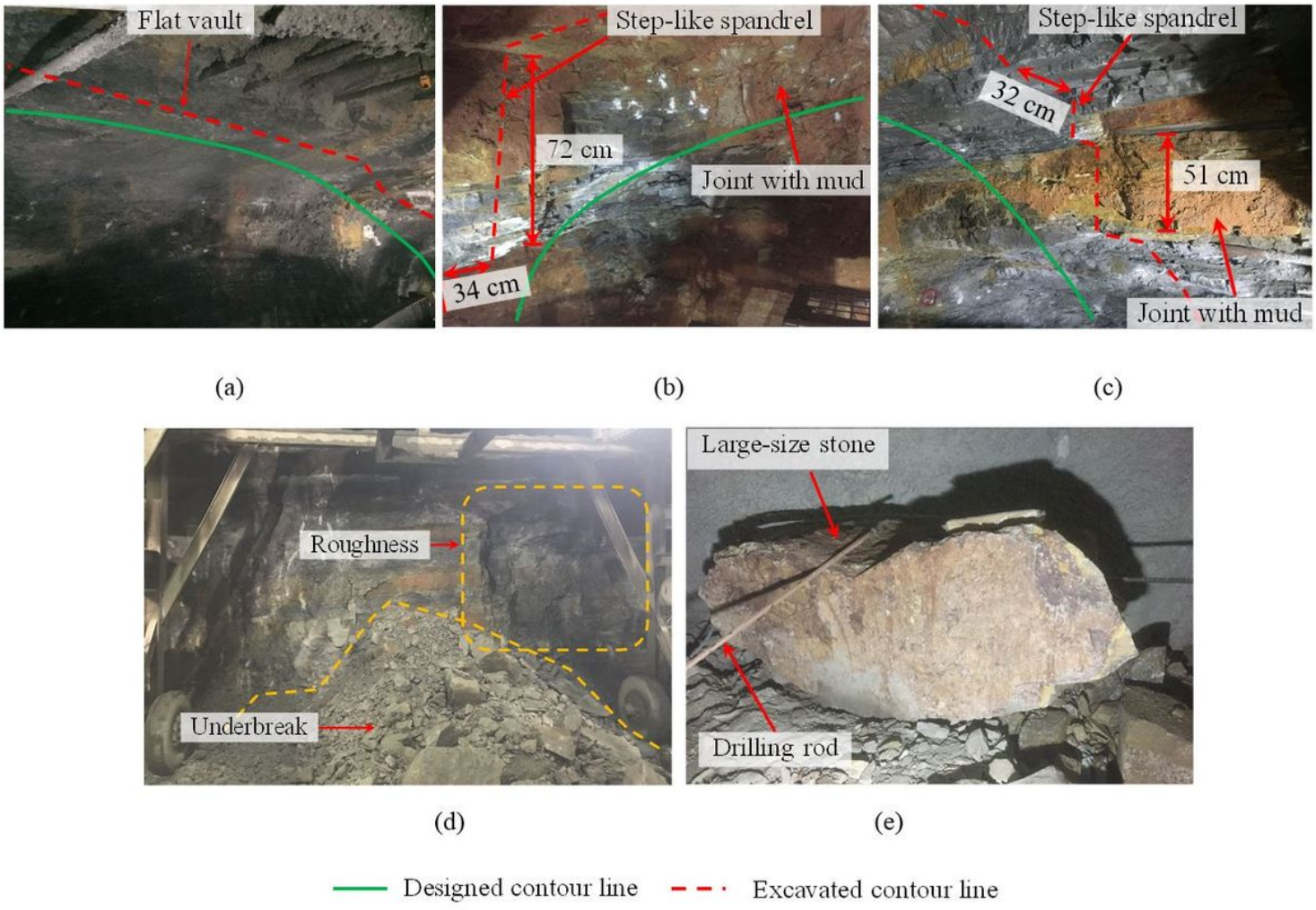

Figure 6

The failure characteristics of horizontal layered surrounding rock after blasting excavation under the original blasting scheme: (a) vault, (b) left spandrel to haunch, (c) right spandrel to haunch, (d) rough face and underbreak, (e) large-size stone

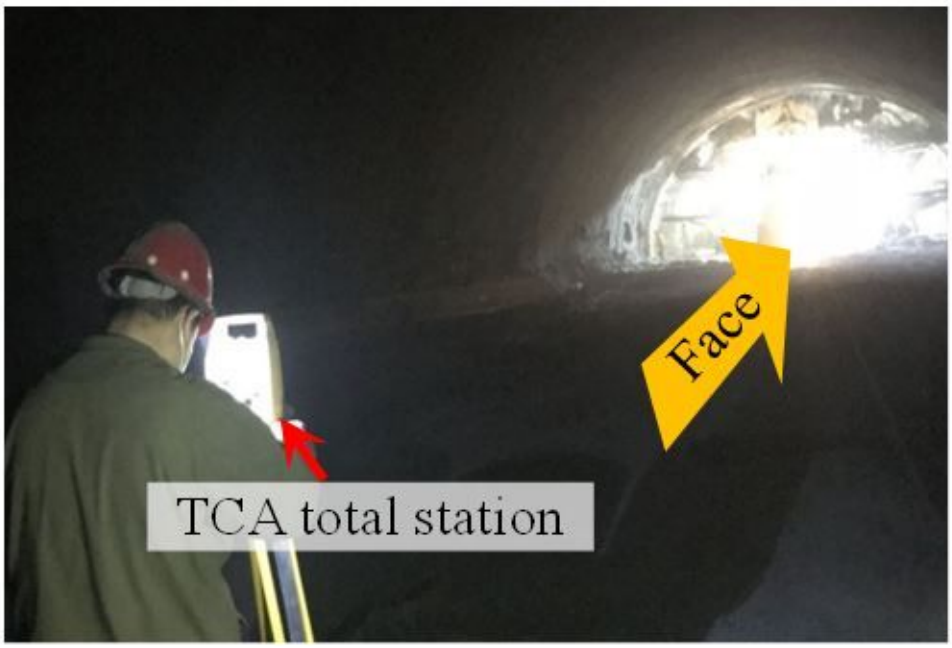

(a)

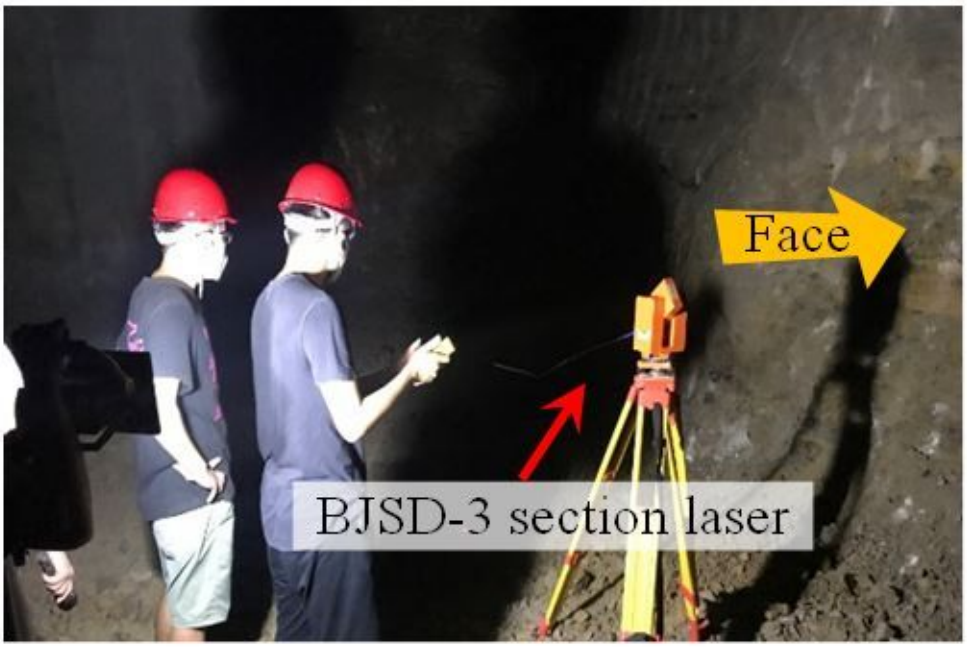

(b)

Figure 7

Field measurements: (a) deformation of surrounding rock and length of each round excavation by using Leica TCA total station, (b) overbreak and underbreak by using BJSD-3 tunnel section laser

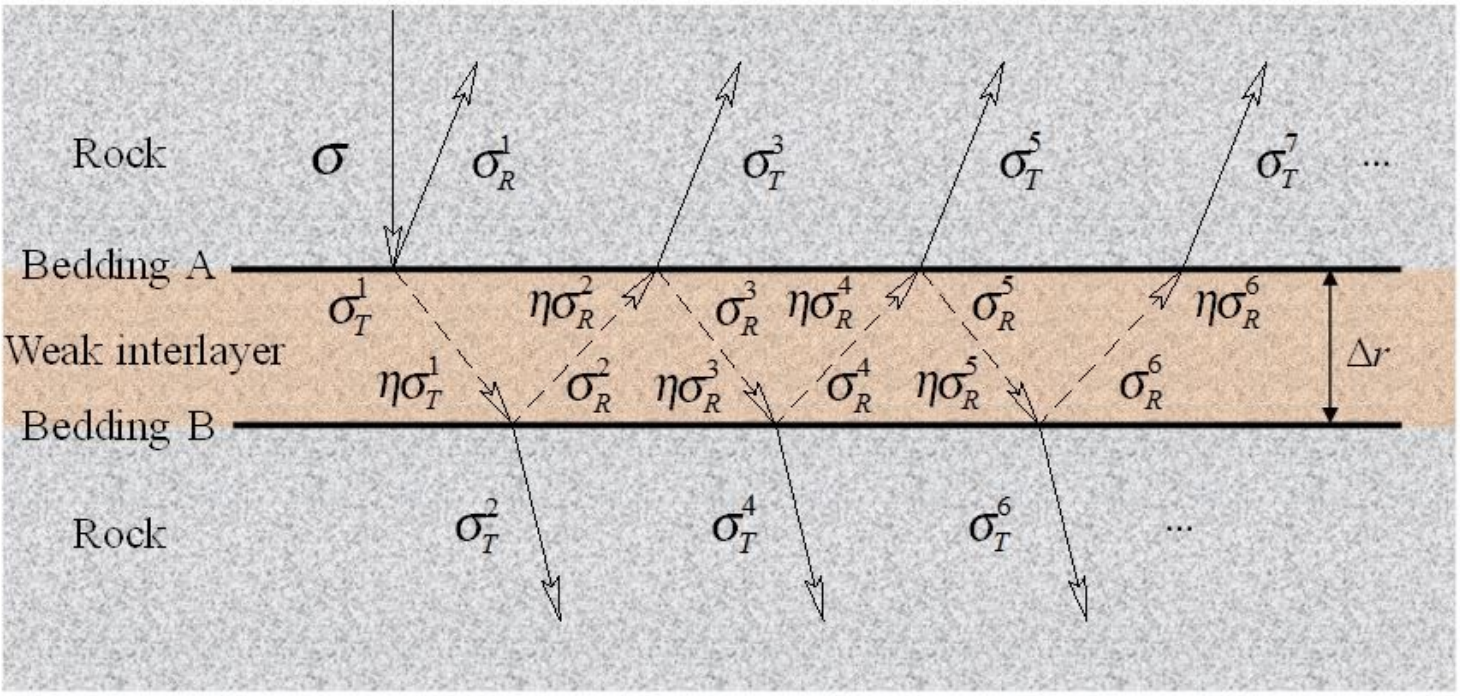

Figure 9

Reflection and transmission of explosive stress wave passing through weak bedding

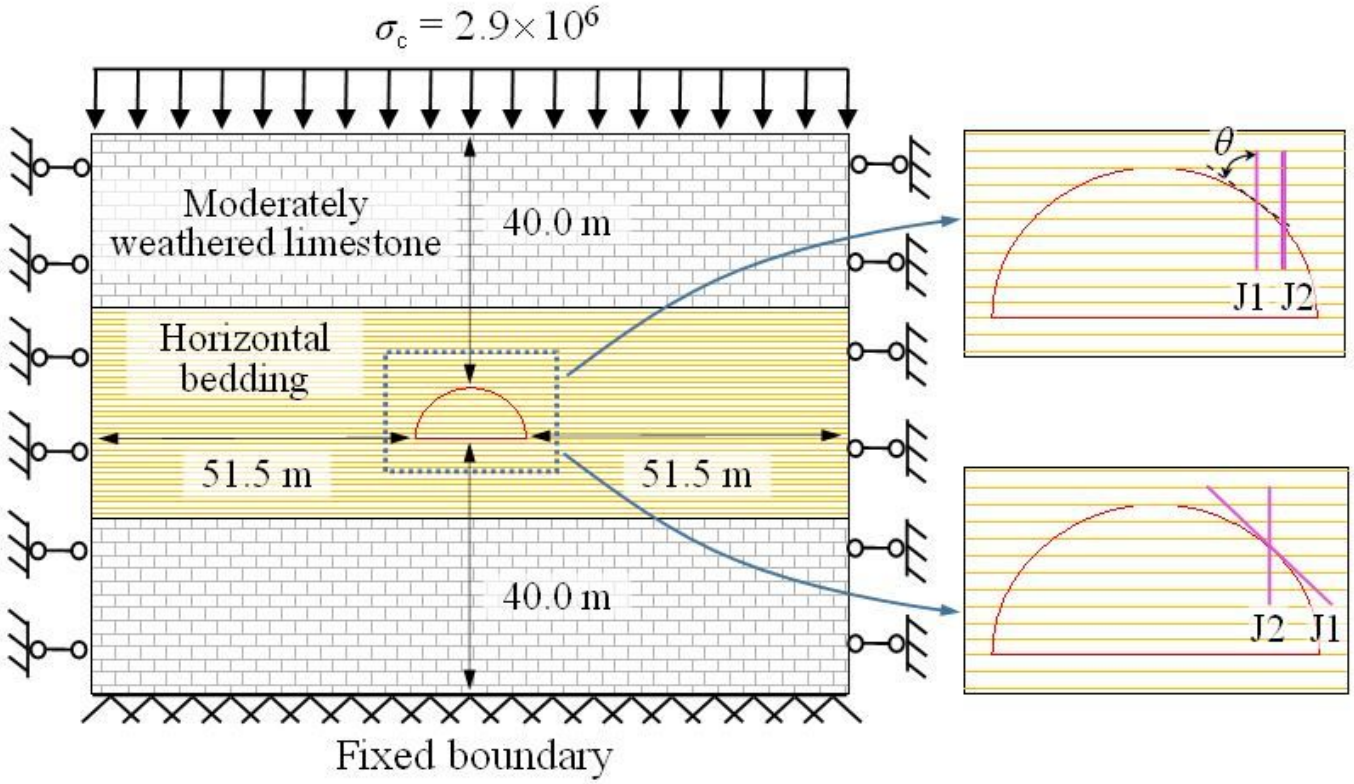

Figure 10

Numerical model of tunnel, and the surrounding rock contains horizontal beddings and two sets of joints

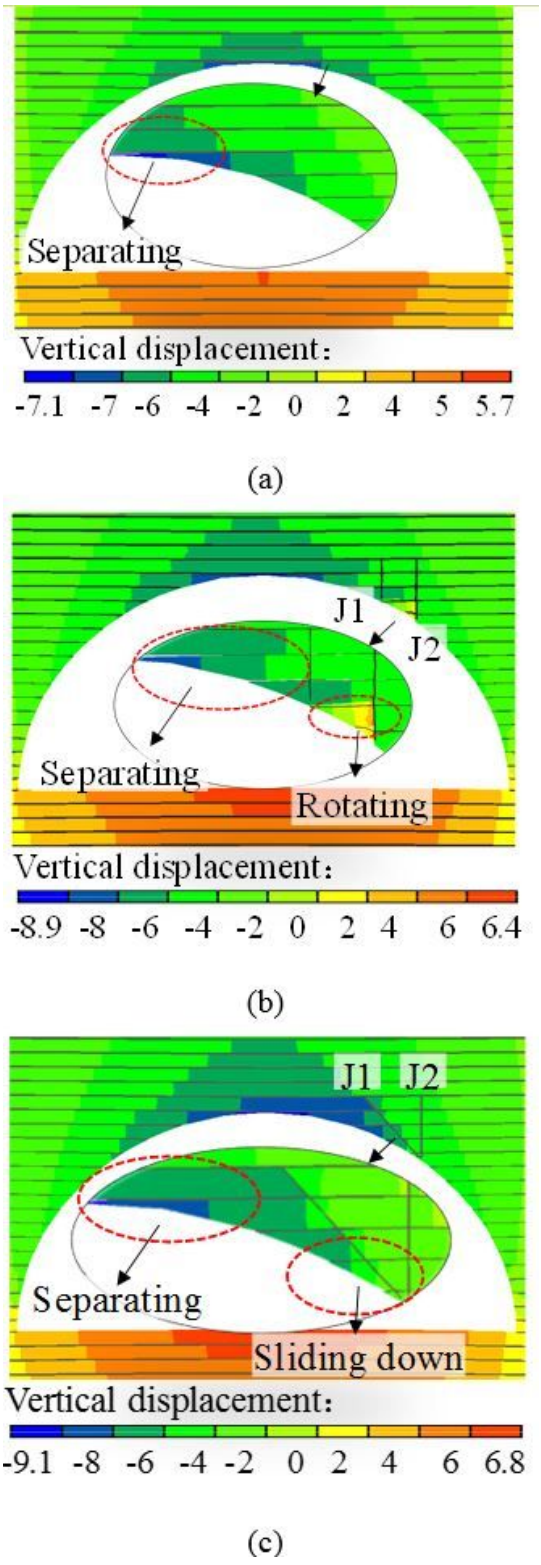

Figure 11

Vertical deformations and failure modes after tunnel excavation: (a) surrounding rock with horizontal beddings, (b) surrounding rock with horizontal beddings and two parallel vertical joints, (c) surrounding rock with horizontal beddings and two sets of intersecting joints

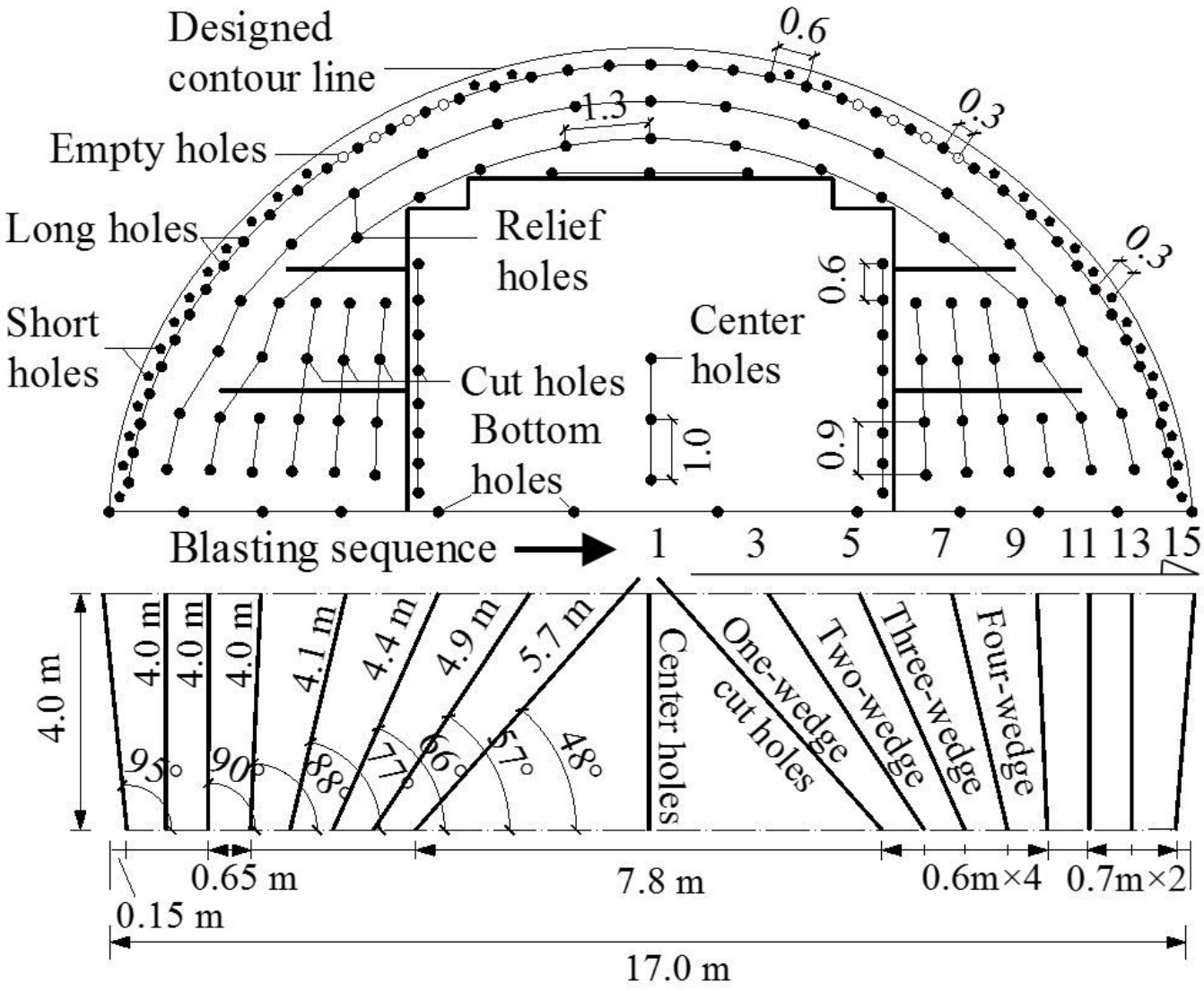

Figure 12

The optimized blasthole pattern and detonator series of the upper face

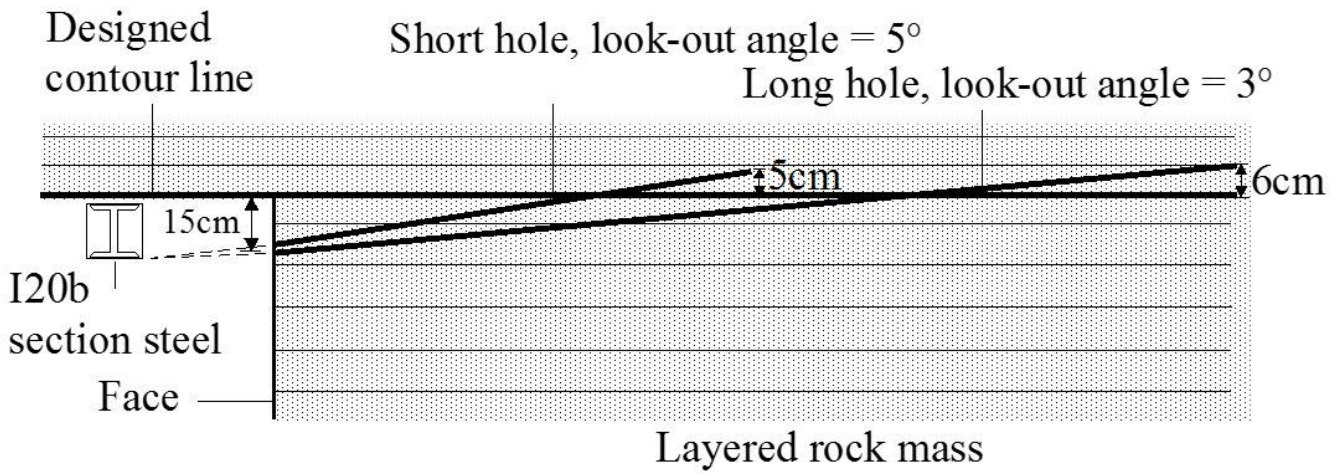

Figure 13

The layout of the optimized peripheral holes

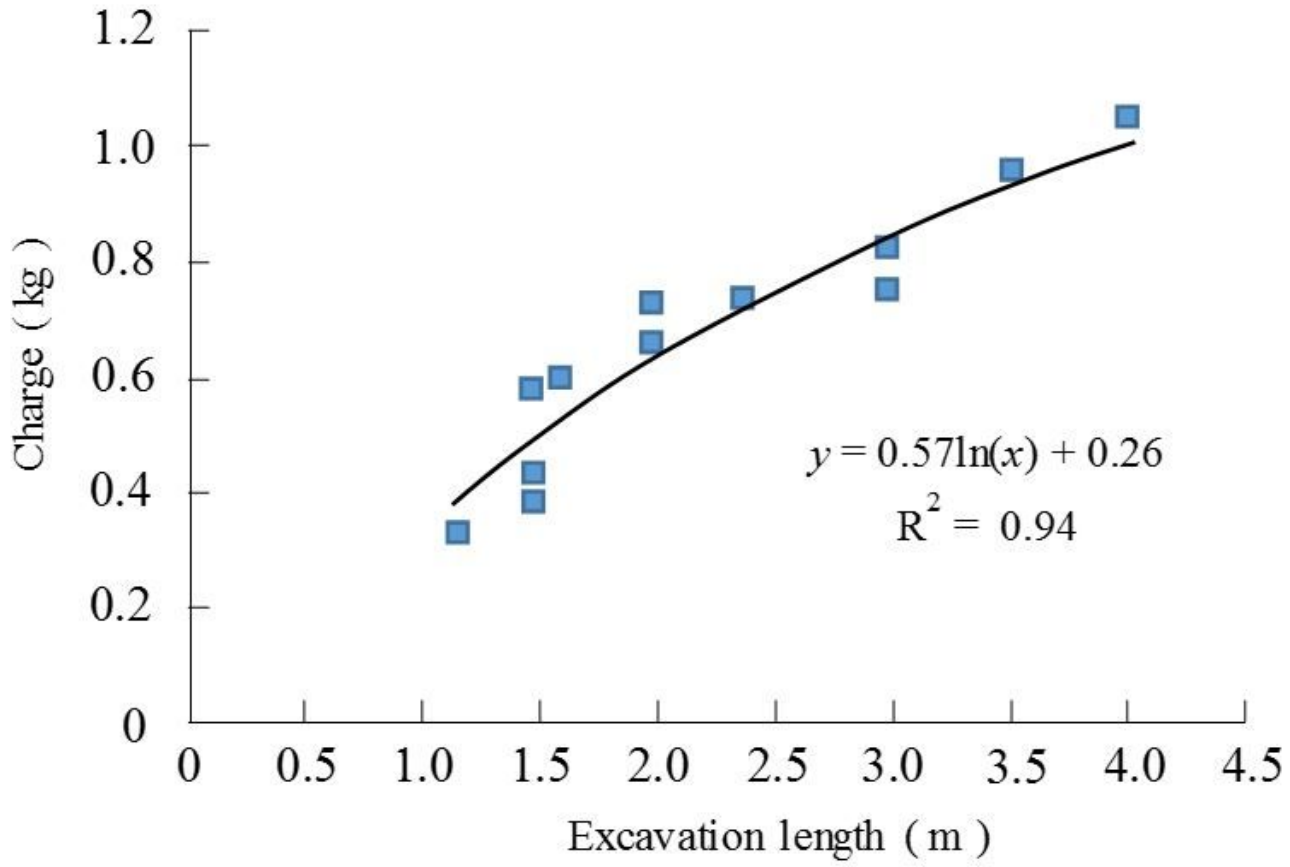

Figure 14

Relation between charge of peripheral hole and each round excavation length

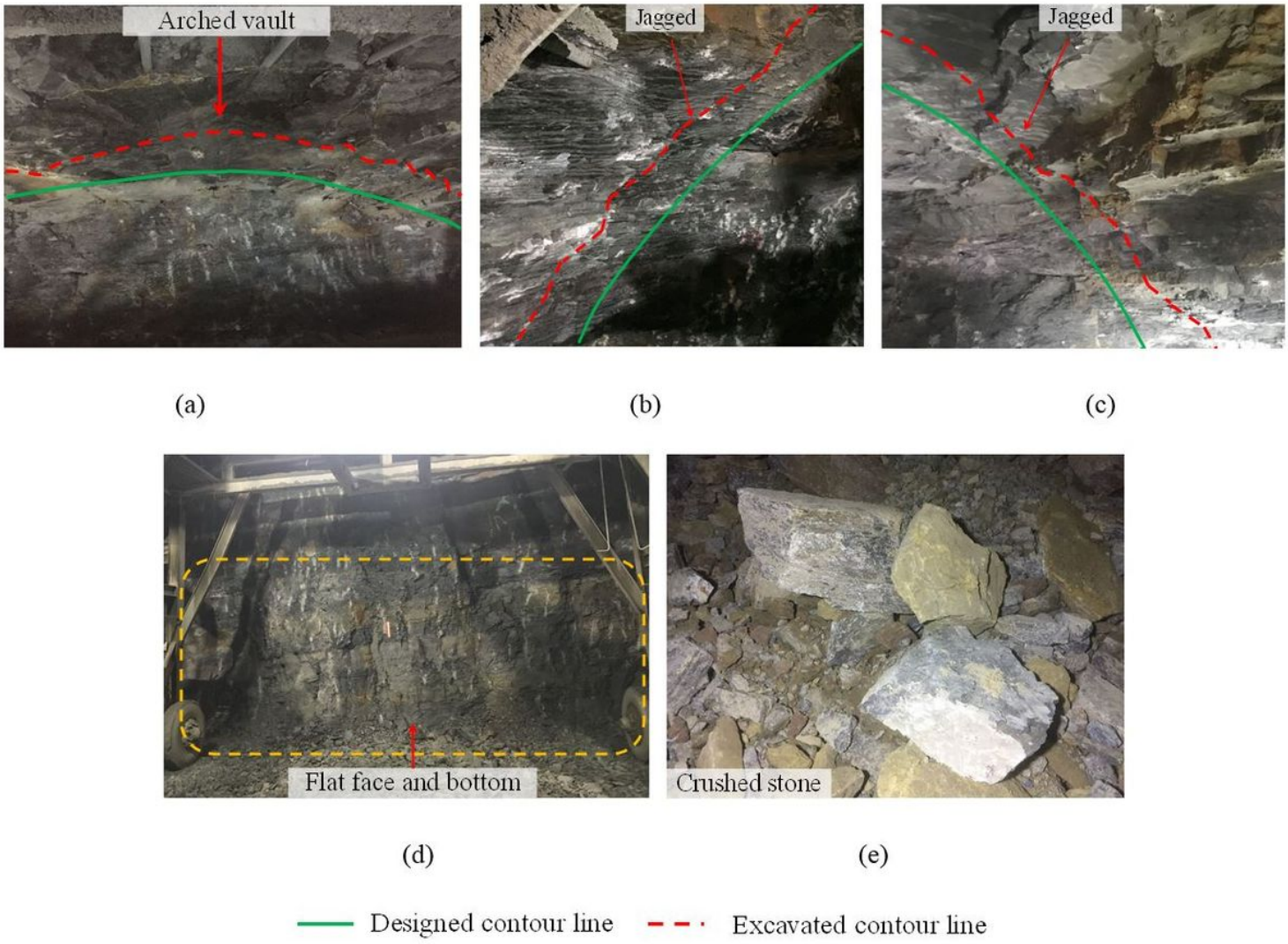

Figure 16

The failure characteristics of horizontal layered surrounding rock after blasting excavation under the optimized blasting scheme: (a) vault, (b) left spandrel to haunch, (c) right spandrel to haunch, (d) flat face and bottom, (e) crushed stones

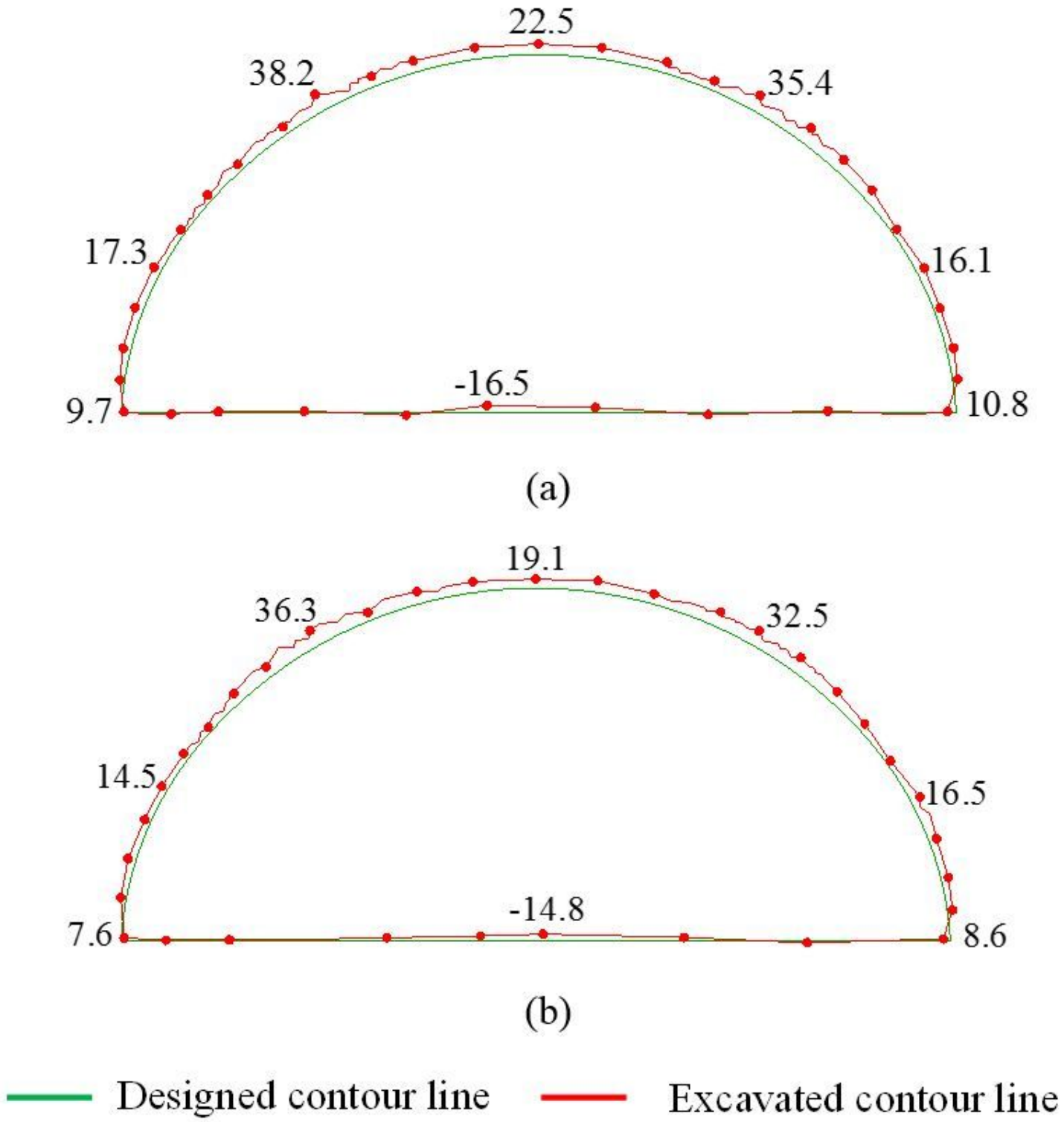

Figure 17

Tunnel overbreak and underbreak of the test sections: (a) ZK80+235.7, (b) ZK80+220.1 (unit: cm)

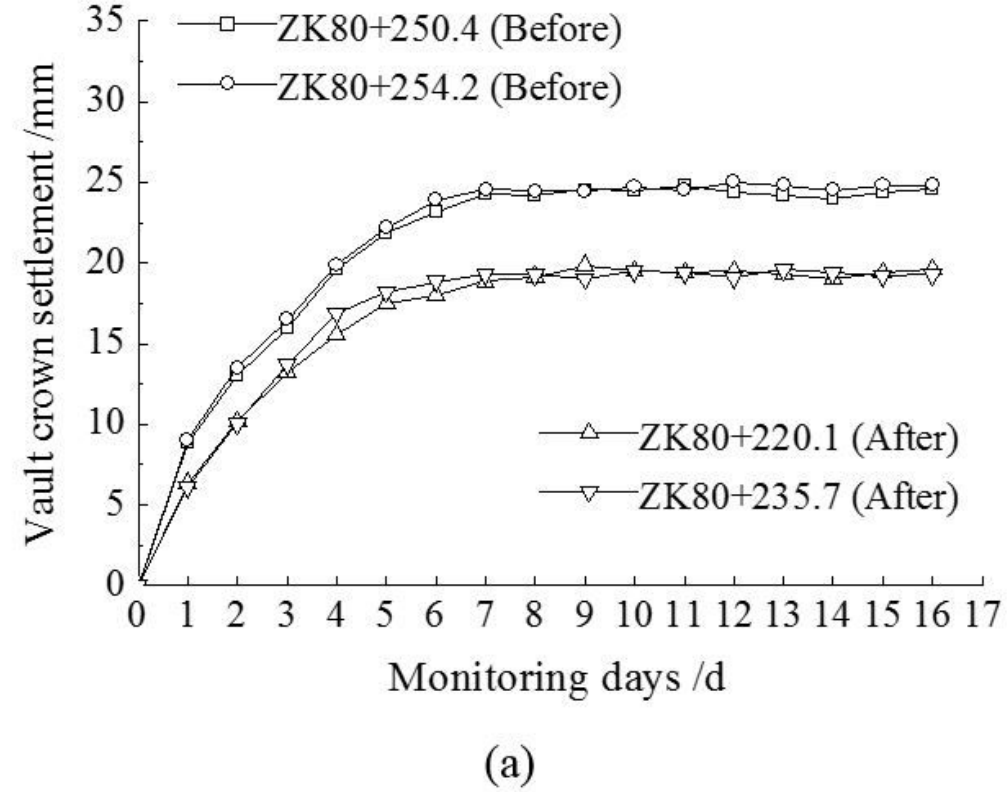

(a)

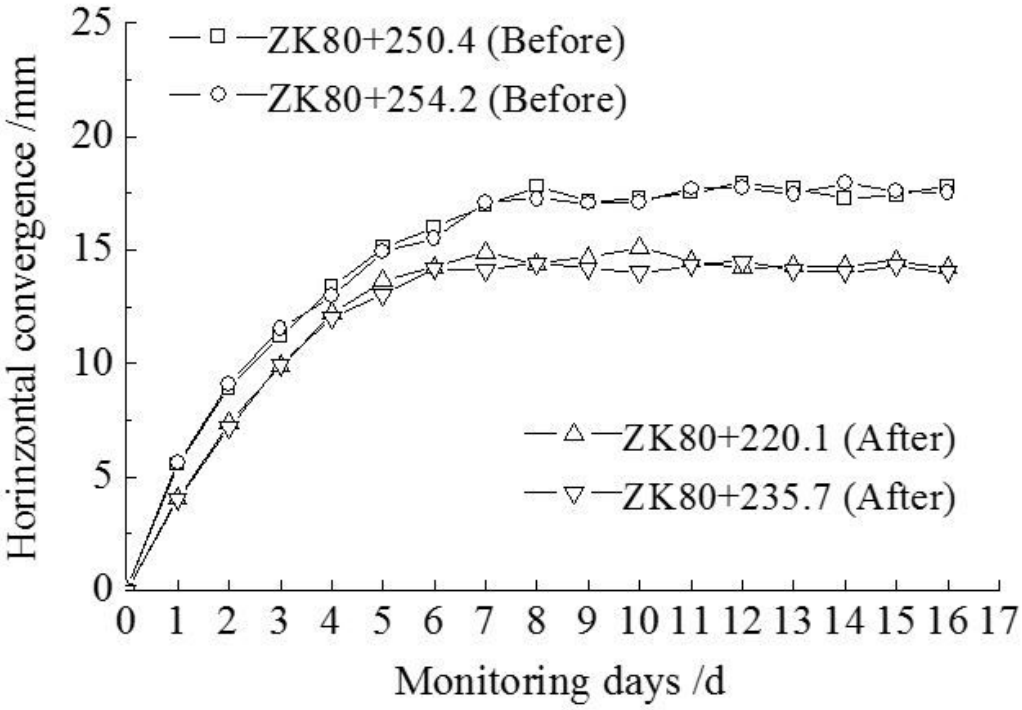

Figure 18

The cumulative displacements of surrounding rock of the test sections: (a) vault crown settlement, (b) haunch horizontal convergence